Structural, NMR Spectroscopic and Computational Investigation of Hemin Loading in the Hemophore HasAp from *Pseudomonas aeruginosa*

Grace Jepkorir[†], Juan Carlos Rodríguez[†], Huan Rui[‡], Wonpil Im[‡], Scott Lovell[§], Kevin P. Battaile[£], Aileen Y. Alontaga[†], Erik T. Yukl[Δ], Pierre Moënne-Loccoz[Δ], and Mario Rivera[*,†]

[†] Department of Chemistry, University of Kansas, Multidisciplinary Research Building, 2030 Becker Dr., room 220 E, Lawrence

[§] Del Shankel Structural Biology Center, University of Kansas, 2034 Becker Dr., Lawrence, KS 66047

[‡] Department of Molecular Biosciences and Center for Bioinformatics, The University of Kansas, Lawrence, Kansas 66047

[Δ] Department of Science and Engineering, Oregon Health & Science University, Beaverton, Oregon 97006

[£] IMCA-CAT, Hauptman-Woodward Medical Research Institute, 9700 South Cass Avenue, Building 435A, Argonne, Il 60439

Abstract

When challenged by low-iron conditions several Gram-negative pathogens secrete a hemophore (HasA) to scavenge hemin from its host and deliver it to a receptor (HasR) on their outer membrane for internalization. Here we report results from studies aimed at probing the structural and dynamic processes at play in the loading of the apo-hemophore secreted by *P. aeruginosa* (apo-HasAp) with hemin. The structure of apo-HasAp shows a large conformational change in the loop harboring axial ligand His32 relative to the structure of holo-HasAp, whereas the loop bearing the other axial ligand, Tyr75, remains intact. To investigate the role played by the axial ligand-bearing loops in the process of hemin capture we investigated the H32A mutant, which was found to exist as a monomer in its apo-form and as a mixture of monomers and dimers in its holo-form. We obtained an X-ray structure of dimeric H32A holo-HasAp, which revealed that the two subunits are linked by cofacial interactions of two hemin molecules and that the conformation of the Ala32 loop in the dimer is identical to that exhibited by the His32 loop in wild type apo-HasAp. Additional data suggest that the conformation of the Ala32 loop in the dimer is mainly a consequence of dimerization. Hence, to investigate the effect of hemin loading on the topology of the His32 loop we also obtained the crystal structure of monomeric H32A holo-HasAp coordinated by imidazole (H32A-imidazole) and investigated the monomeric H32A HasAp and H32A-imidazole species in solution by NMR spectroscopy. The structure of H32A-imidazole

[*]To whom correspondence should be addressed: mrivera@ku.edu.

revealed that the Ala32 loop attains a "closed" conformation nearly identical that observed in wild type holo-HasAp, and the NMR investigations indicated that this conformation is maintained in solution. The NMR studies also highlighted conformational heterogeneity at the H32 loop hinges and in other key sections of the structure. Targeted molecular dynamics simulations allowed us to propose a possible path for the closing of the His32 loop upon hemin binding and identified molecular motions that are likely important in transmitting the presence of hemin in the Tyr75 loop to the His32 loop to initiate its closing. Importantly, residues implicated as undergoing motions in the computations are also observed as being dynamic by NMR. Taken together, these observations provide direct experimental evidence indicating that hemin loads onto the Tyr75 loop of apo-HasAp, which triggers the closing of the His32 loop.

INTRODUCTION

The preferred aerobic metabolism of *Pseudomonas aeruginosa* requires enzymes that incorporate iron as cofactor. Availability of the nutrient in host organisms, however, is scarce because most of the total body iron is intracellular and not readily available to an invading pathogen.[1] Iron limitation causes stress response in pathogens that triggers deployment of several iron acquisition systems,[2,3] which fall in four categories, (*i*) excretion of low-molecular weight iron ligands (siderophores) and the corresponding receptors for the intake of iron-loaded siderophores, (*ii*) direct binding of iron-containing host proteins at outer membrane receptors which internalize only iron, (*iii*) direct binding of heme at outer membrane receptors which internalize the macrocycle, and (*iv*) secretion of heme binding proteins (hemophores) that work in pairs with receptor proteins for heme internalization. The investigations reported herein, which address possible steps for loading hemin into a hemophore secreted by *P. aeruginosa* are concerned with the latter category. To capture heme *P. aeruginosa* also secretes hemolysins that rupture red blood cells and release hemoglobin,[4] which together with the secreted hemophores increase the efficiency of heme capture. *P. aeruginosa* deploys two heme uptake systems, *phu* (**P**seudomonas **h**eme **u**ptake)[2] and *has* (**h**eme **a**cquisition **s**ystem);[5] the latter consists of an outer membrane heme receptor (*hasR*) and a protein that binds hemin, also known as the hemophore HasAp. The latter is similar to a hemophore secreted by *Serratia marcescens* (HasAs),[6] which is known to bind hemin with high affinity ($\sim 5 \times 10^{10}$ M)[7] for subsequent delivery to the receptor HasR on its outer membrane.[8] The gene coding for HasAp has been shown to be upregulated under iron limiting conditions and essential for growth of *P. aeruginosa* with hemoglobin as the only source of iron[9], observations that point to a vital role in the capture and subsequent utilization of heme iron.

Hemin-loaded HasAs[10,11] and HasAp[12] have been shown to share identical structures composed of an "α-helix wall" packed against a "β-sheet wall"; together both "walls" form a structure from which two extended loops stem (Figure 1). These two loops harbor the ligands (His32 and Tyr75) that coordinate the heme iron axially; Tyr75 engages in a hydrogen bond interaction with conserved His83, which appears to enhance the phenolate character of the Tyr75 ligand.[10,12] The loops harboring each of the axial ligands will be referred to as His32 loop and Tyr75 loop hereafter. A solution NMR structure of apo-HasAs showed a large conformational rearrangement of the His32 loop that relocates the His32 ligand approximately 30 Å from its position in the holo-protein, while the Tyr75 loop and the rest of the structure remain virtually unaffected.[13] Replacing Tyr75 with Ala in HasAs causes a nearly two order of magnitude decrease of the heme binding affinity, while replacing His32 with Ala causes a decrease of approximately 5-fold;[7] the nature of the ferric heme-iron coordination or the structure of these mutants has not been reported. Addition of dithionite to holo-HasAs in the presence of CO results in formation of a ferrous hexacoordinate complex axially ligated by Tyr75 and CO,[14] which suggest that His32 is the

more labile axial ligand in the reduced hemophore. That His32 is also more labile than Tyr75 in the ferric state finds support in crystal structures of HasAs in complex with its receptor (HasR), where hemin in the hemophore is axially coordinated only by Tyr75, while the His32 loop is disordered.[15] Together, these observations have been used to hypothesize a two-step mechanism where hemin is initially loaded onto the Tyr75 loop, followed by closure of the His32 loop, which is mediated by coordination of His32 and formation of hydrogen bonds between hemin propionate and key residues in the His32 loop.[13] This mechanism, if operative, would be distinct from that elucidated for the Shp hemophore secreted by the Gram-positive *Streptococcus pyogenes*,[16] which binds hemin with two axial Met ligands[17] without detectable intermediates.[18]

As part of our efforts to understand the structures, dynamics and intermolecular interactions of several *P. aeruginosa* proteins involved in heme-iron uptake and metabolism, our laboratories have been working toward elucidating the mechanism of hemin loading onto the hemophore HasAp. In a recent study it was shown that binding of free hemin is characterized by an initial rapid kinetic phase that leads to formation of a high-spin ferric hemin intermediate, which is followed by a slower phase that culminates in formation of a low-spin ferric complex where hemin is bound by His32 and Tyr75.[19] Importantly, monitoring the same reaction in the H32A-HasAp variant only revealed the rapid phase to form a stable hemin-protein complex equivalent to that of the wild-type intermediate.[19] These results represent the first documented kinetic evidence supporting a two-step binding model in which hemin is thought to bind rapidly to the Tyr75 loop, followed by slower closure of the His32 loop. In this report we document biochemical, structural and NMR spectroscopic evidence demonstrating that hemin binds to Tyr75, triggering relocation of the His32 loop from its position in the apo HasAp structure to a position very similar that adopted in the holo HasAp structure, even if His32 coordination is not possible, as this residue was replaced by a non-coordinative Ala. The presence of hemin in the Tyr75 loop is likely transferred to the His32 loop via an enhanced dynamic behavior of helix α2 and a short loop connecting it to α3. Molecular dynamics simulations that capitalized on the availability of structures for hemin-free and hemin loaded HasAp provide additional insight into molecular motions that relay the presence of hemin in the Tyr75 loop to the His 32 loop and suggest a possible path for its relocation upon hemin binding.

EXPERIMENTAL METHODS

Protein Expression and Purification

A gene coding for a truncated form of HasAp missing the last 21 C′-terminal amino acids relative to the full-length protein was constructed as described previously.[12] The H32A mutation was introduced by site directed mutagenesis using the QuickChange mutagenesis kit (Stratagene) and the mutation confirmed by DNA sequencing (SeqWright) prior to transforming the plasmid into *E. coli* BL 21 GOLD (DE3) competent cells. An overnight starter culture of 50 mL Luria-Bertani (LB) medium (100 μg/mL ampicillin) was grown from a single colony; 30 mL of the culture was used to inoculate 1 L of M9 minimal medium[20] containing 200 μg/mL ampicillin. Cells were grown to an OD_{600} of 0.8–0.9 then collected by centrifugation at 4800 rpm for 10 min at 4 °C. The pelleted cells were resuspended in 1 L of fresh minimal M9 medium (200 μg/mL ampicillin) and cultured at 37 °C to an OD_{600} of ~0.9. The temperature was lowered to 30 °C with continuous incubation to an OD_{600} of ~1.0 and protein expression was induced by the addition of isopropyl β-D-thiogalactopyranoside (IPTG) to a final concentration of 1 mM. The cells were cultured for 5 h before they were harvested and stored at −20 °C. The cell pellet was resuspended in 20 mM Tris-HCl (pH 7.6) (3 mL/g cell paste), and disrupted by sonication in the presence of DNase (Sigma-Aldrich, St. Louis, MO); the cell debris were separated by centrifugation at 19,500 rpm at 4 °C for 40 min.

Purification of Apo-Proteins

Purification of apo- wild type HasAp or its H32A mutant was carried out by ion exchange chromatography (IEC) at 4 °C and by hydrophobic interaction chromatography (HIC) at ambient temperature: Specifically, the clarified supernatant was loaded onto a Q-Sepharose Fast Flow column (2.6 cm i.d. × 15 cm; GE Healthcare) equilibrated with 20 mM Tris-HCl (pH 7.6) The column was then washed with at least 3 bed volumes of the same buffer and the protein was eluted with the same buffer and a linear gradient (0–600 mM) of NaCl. Fractions containing HasAp were pooled and dialyzed against 50 mM sodium phosphate buffer containing 0.7 M ammonium sulfate (pH 7.0) prior to loading onto a Butyl Sepharose Fast Flow (GE Healthcare) column (2.6 cm i.d. × 12 cm) equilibrated with the same buffer. Protein was eluted in two stages: (*i*) 50 mM sodium phosphate/0.5 M ammonium sulfate, pH 7.0 was used to elute weakly bound proteins and holo-HasAp, and (*ii*) a linear gradient of sodium phosphate buffer (50 mM–20 mM)/ammonium sulfate (0.50 M – 0 M) was used to elute apo-HasAp. Fractions containing the apo-protein were loaded onto a Phenyl Sepharose 6 Fast Flow high substitution (GE Healthcare) column (2.6 cm i.d. × 12 cm) and eluted using steps (*i*) and (*ii*) described above. The purity of the protein in the resultant fractions was assessed by SDS-PAGE and if necessary, fractions containing apo-HasAp were purified again on a second Butyl Sepharose column. The MW of apo-wild type and H32A apo-HasAp was determined by electrospray mass spectrometry and the degree of oligomerization (monomer/dimer) was determined in solution with the aid of a high-resolution gel filtration column (Superdex™ 75 prep grade, GE Healthcare) equilibrated with 50 mM Tris-HCl (pH 7.5), 100 mM KCl. The column was calibrated with cytochrome *c* (12.4 kDa.), chymotrypsin (25 kDa.), ovalbumin (44 kDa.), and albumin (67 kDa.).

Preparation of H32A Holo-HasAp

1.8–2.0 μmoles of apo-protein (8–10 μM) in sodium phosphate buffer (μ= 0.1, pH= 7.8) was reconstituted with hemin (1.0 mM) dissolved in dimethyl sulfoxide (DMSO) by titration under constant stirring until the absorbance ratio (A_{280}/A_{402}) remained constant. The resultant holo-protein was incubated overnight at 4 °C, concentrated to 2 mL using 10 kDa MWCO Amicon ultracentrifuge filter devices and passed through a G-75 Sephadex column (2.6 cm i.d. × 90 cm; GE Healthcare) equilibrated with phosphate buffer (μ= 0.1, pH= 7.8).

Expression and Purification of Isotopically Labeled Proteins

Uniformly labeled, U-^{15}N-H32A HasAp and U-^{13}C/U-^{15}N-HasAp, were prepared using a minor modification of the above-described protocol: Cells were resuspended in M9 containing 1.0 g ^{15}NH$_4$Cl for preparing U^{15}N-H32A HasAp or in M9 containing 1.0 g ^{15}NH$_4$Cl and 2.0 g ^{13}C$_6$-D-glucose for preparing U-^{13}C/U-^{15}N-H32A-HasAp. Samples selectively labeled with ^{15}N-Gly, ^{15}N-Ala, or ^{15}N-Val were prepared with the above-described protocols supplementing the M9 media according to previously reported procedures.[21−23]

Resonance Raman (RR) and EPR Spectroscopy

RR spectra were obtained using a custom McPherson 2061/207 spectrograph (0.67 m with variable gratings) equipped with a Princeton Instruments liquid N$_2$-cooled CCD detector (LN-1100PB). Excitation at 413 nm was provided by a krypton laser (Innova 302, Coherent), and a Kaiser Optical supernotch filter was used to attenuate Rayleigh scattering. Spectra at room temperature were collected in a 90° scattering geometry on samples mounted on a reciprocating translation stage. Frequencies were calibrated relative to indene and CCl$_4$ and are accurate to ±1 cm^{-1}. CCl$_4$ was also used to check the polarization conditions. The integrity of the RR samples, before and after laser illumination, was confirmed by direct monitoring of their UV-vis spectra in the Raman capillaries. Low

temperature spectra were obtained in a backscattering geometry on samples maintained at ~ 105 K in a liquid nitrogen cold finger. Frequencies were calibrated relative to aspirin and are accurate to ± 1 cm^{-1}. EPR spectra were obtained on a Bruker E500 X-band EPR spectrometer equipped with a superX microwave bridge and a dual mode cavity with a helium-flow cryostat (ESR900, Oxford Instruments, Inc.). The experimental conditions, *i.e.*, temperature, microwave power, and modulation amplitude, were varied to optimize the detection of all potential EPR active species and to ensure non-saturating conditions.

Crystallization

Search for optimum crystal growth conditions was conducted using the sitting drop vapor diffusion method in Compact Jr. Crystallization plates (Emerald BioSystems) at 20 °C. Equal volumes of protein and crystallization solution were mixed and equilibrated against 100 μL of reservoir solution. Crystals of apo-HasAp, approximately 300 μm in length and displaying a needle morphology were obtained after 1–2 days from 50 mg/mL protein in 100 mM sodium phosphate pH 7.8, and Wizard 2 (Emerald BioSystems) condition #19 (1.6 M NaH$_2$PO$_4$/0.4 M K$_2$HPO$_4$, 100 mM phosphate-citrate pH 4.2). Samples were transferred to a solution containing 80% crystallization solution and 20% glycerol for approximately 30 seconds before freezing in liquid nitrogen for data collection. Prismatic crystals of dimeric H32A holo-HasAp approximately 700 μm in the longest direction were obtained within 24 hours from 15 mg/mL protein in sodium phosphate, pH 7.0, and Wizard 2 condition #15 (1.26 M (NH$_4$)$_2$SO$_4$, 100 mM HEPES pH 7.5). Crystals were transferred and equilibrated for 60 s in a solution containing 2 M NH$_4$SO$_4$, 100 mM HEPES pH 7.5, 10% d-sorbitol and then in the same solution containing 20% d-sorbitol before freezing in liquid nitrogen. Prismatic crystals of imidazole bound H32A holo-HasAp were obtained after approximately 4 weeks from 9.3 mg/mL protein in 150 mM imidazole pH 7.0, and Wizard 2 condition #34 (10% (w/v) PEG 8000, 100 mM imidazole pH 8.0). Samples were transferred to a solution containing 80% crystallization solution and 20% (v/v) PEG 400 before freezing in liquid nitrogen.

X-ray data collection, structure solution and refinement

Data for apo- and dimeric holo-HasAp were collected at 100 K at the Advanced Photon Source (APS) IMCA-CAT, beamline 17BM using an ADSC Quantum 210r CCD detector. Diffraction data for imidazole bound H32A holo-HasAp were collected at 93 K in-house using a Rigaku RU-H3R rotating anode generator equipped with Osmic Blue focusing mirrors and an R-axis IV^{++} image plate detector. Apo-HasAp and imidazole bound H32A holo-HasAp diffraction data were integrated and scaled with the HKL2000 package[24] and dimeric H32A holo-HasAp data were processed with the XDS[25] package. The Laue class for each data set was checked using Pointless.[26] Structure solution of apo-HasAp was obtained by molecular replacement with Molrep[27] using the holo-HasAp structure (PDB: 3ELL)[12] as the search model. Automated model building was conducted with ARP/wARP.[28] The final model was used for subsequent molecular replacement searches with the dimeric H32A holo-HasAp and imidazole bound H32A holo-HasAp data sets. Structure refinement was performed with Refmac[29] for apo and imidazole bound holo H32A HasAp and with Phenix[30] for dimeric H32A holo-HasAp, respectively. Manual model building was carried out with Coot.[31] The crystals of dimeric H32A holo-HasAp were indexed in a monoclinic *C* lattice with $a = 110.34$ Å, $b = 52.70$ Å, $c = 71.74$ Å, $\beta = 129.05$ ° and space group *C*2. However, the unit cell and space group were transformed to the non-standard setting *I*2 using the reindexing matrix (0 0 −1, 0 1 0, 1 0 1) to give $a = 71.74$ Å, $b = 52.70$ Å, $c = 85.71$ Å, $\beta = 91.48°$. For dimeric H32A holo-HasAp, anisotropic displacement parameters were modeled by TSL refinement[32] using 10 and 11 TLS groups for subunits A and B respectively. Molecule B appeared to display increased thermal motion as indicated by the larger overall B-factor (~2-fold) relative to molecule A. For the imidzole bound H32A holo-

HasAp, 7 TLS groups were refined for both molecules of the non-crystallographic dimer in the asymmetric unit. Structure validation was performed using MOLPROBITY[33] and figures were prepared using CCP4mg.[34] Relevant crystallographic data are provided in Table 1. For apo-HasAp, phosphate and a sodium ions were identified from the difference electron density and assigned based on the coordination and expected non-bonded distances; [35] their location in the structure is shown in Supplementary Figure S1.

NMR Spectroscopy

Sequential backbone resonance assignments were obtained with the aid of ^{1}H-^{15}N-HSQC, HNCA, HN(CO)CA, HNCACB, CBCA(CO)NH, HNCO, and HN(CA)CO experiments conducted with H32A HasAp samples uniformly labeled with ^{13}C and ^{15}N, at protein concentrations that ranged between 3.9 mM and 6.7 mM in phosphate buffer ($\mu = 0.1$, pH 7.0) with 5–10 % D_2O. After collecting the data necessary to carry out resonance assignments of H32A HasAp, the same sample was subjected to 3 cycles of buffer exchange using 10 KDa MWCO Amicon Ultra-15 centrifugal filter devices, replenishing the solution with 100 mM imidazole, pH 7.0 buffer after every concentration step. The solutions of thus prepared H32A-imidazole samples were finally concentrated to the same volume of the original H32A HasAp sample in order to maintain the protein concentration constant. Samples of ^{15}N-Gly (4.6 mM), ^{15}N-Ala (4.4 mM), and ^{15}N-Val (5.2 mM) selectively labeled proteins were used to collect two-dimensional ^{1}H-^{15}N-HSQC spectra using standard and rapid repetition conditions. For rapid repetition HSQC experiments, the acquisition time and relaxation delay were shortened to 35 ms and 50 ms, respectively from the standard 95 ms and 1s, and the number of scans was increased to at least 256 from the typical 16 scans per increment used in standard experiments. All other acquisition parameters were identical. The temperature was 32 °C unless otherwise noted. Other pertinent acquisition and processing parameters used to obtain specific spectra are included in the corresponding figure caption. All experiments were conducted using a Varian Unity Inova 600 NMR spectrometer equipped with a triple resonance probe. The data were processed using NMRPipe[36] and analyzed with the program Sparky.[37] ^{1}H chemical shifts were referenced directly to internal DSS using the methyl ^{1}H resonance at 0.00 ppm, whereas ^{15}N and ^{13}C chemical shifts were referenced indirectly using the ratio of gyromagnetic ratios.

Targeted Molecular Dynamics (TMD) Simulations

All calculations were performed using the biomolecular simulation program CHARMM[38] with the all-atom parameter set PARAM22 for proteins,[39] including the dihedral cross-term corrections (CMAP)[40] and a modified TIP3 water model.[41] The simulation system, shown in Supplementary Figure S2, was built by using the *Quick MD Simulator* module in CHARMM-GUI[42] after the hemin-iron was coordinated to the phenol group of Tyr75 in the structure of apo-HasAp. Holo-HasAp was solvated in a 80 Å × 80 Å × 80 Å water box with 0.15 M KCl, resulting in a total of 48,292 atoms; the number of water molecules, K^+ and Cl^- ions are 15,191, 50 and 37, respectively; different numbers of K^+ and Cl^- ions were added to make the simulation system neutral. After 350 ps equilibration time, 25 independent 1.2 ns TMD simulations were performed starting from the "open" (apo) and progressing to the "closed" (holo) structure. A time step of 2 fs was used for the NVT (constant volume and temperature) dynamics with the SHAKE algorithm.[43] The same options as in the input scripts provided by CHARMM-GUI were used for non-bonded interactions.[42] A total of 50 structures ("images") were generated at equal intervals of root mean squared deviation (RMSD) between the open and closed structures for each run, followed by clustering the images obtained at each of the RMSD intervals. Analysis of the trajectories was also performed to identify important interactions during the transition from "open" to "closed" structures.

RESULTS

Purification of the Apo-Proteins

Expression of wild type (wt) or H32A HasAp in *E. coli* produces a mixture of holo- and apo-protein in approximate proportion of 1:4. Previous preparations of holo-HasAp addressed this issue by reconstituting the apo-protein during the purification process.[12] Initial preparations of apo-HasAp were obtained upon extraction of the hemin utilizing the cold acid-acetone method, as reported for the preparation of apo-HasAs.[8] In the case of HasAp, extraction of the hemin is incomplete, leaving approximately 3–10% holo-protein contaminating the apo-protein preparations. To overcome this issue we developed a chromatographic method for the separation of apo- and holo-HasAp which capitalizes on the tenacious binding of the apo-protein to hydrophobic affinity interaction columns, relative to the holo-protein. This approach allows complete separation of the holo-form and gentle isolation of the apo-protein for subsequent crystallographic and NMR spectroscopic studies. The molecular mass of wild type and H32A apo-proteins was determined by electrospray ionization mass spectrometry; the experimental values, $18,760 \pm 1$ Da for wt apo-HasAp and $18,690 \pm 1$ Da for the H32A mutant, are in good agreement with the 18,759 and 18,690 Da calculated from the corresponding amino acid sequences, without the initiator methionine.

Structural Characterization of Apo-HasAp

The fold of wt apo-HasAp is very similar to that of its holo-counterpart, with exception of the His32 containing loop, which is significantly displaced from its position in the structure of wt holo-HasAp (3ELL).[22] As can be seen in the structural alignment of the apo- and holo-HasAp structures (Figure 2-A), the "β-sheet wall" comprised of eight antiparallel β-strands connected by short turns and the "α-helix wall" opposite to the "β-sheet wall" are nearly identical. The structure of the loop containing axial ligand Tyr75 (Tyr75 loop) is also highly conserved between holo- and apo-HasAp; in contrast, the loop containing axial ligand His32 (His32 loop) undergoes large reorganization upon binding hemin. The RMSD deviation of C_α atoms (Ser2 to Ala183) between apo- and holo-HasAp (PDB: 3ELL), not including residues Gly28 to Gly45 of the H32 loop, is 0.592 Å. The comparison was made using the Superpose[44] alignment tool in the CCP4 software package. Similar large changes of the His32 loop were observed upon comparing the X-ray[10] and solution state NMR[13] structures of apo-HasAs, which indicates that the large reorganization of the His32 loop upon hemin binding is very likely a common feature of hemin capture by equivalent hemophores from different bacteria. Moreover, comparison of amino acid sequence to other hemophores (Figure 3) in the context of a structural alignment of apo- and holo-HasAp shows that most of the conserved residues are hydrophobic and they function by providing a network of stabilizing hydrophobic interactions in the α-helix and β-sheet walls. Several conserved residues are located near the "hinges" at each end of the His32 loop (Gly28 to Gly 45) and in the Tyr75 loop (His74 to Leu85). It is noteworthy that one of the axial ligands to the hemin iron, His32, is not conserved and that there are no conserved residues in the stretch of sequence spanning the His32 loop.

As can be seen in Figure 2-B the "hinges" about which the His32 loop pivots are located at Gly28 (C′-end of α1) and at Gly45 (the beginning of β2); Gly28 is present in all sequences shown in Figure 3 except in *Pseudomonas entomophila*, and residue 45 is Gly in all sequences except those of *Yersinia pseudotuberculosis, Y. pestis,* and *Y. pestis antiqua*, where it is Ser. Notably, conserved aromatic residues are located near both "hinge" residues; Phe27 is near hinge residue Gly28 and Phe46 is near hinge residue Gly45. The side chain of Phe27, located at the end of α1 packs against the side chain of conserved Trp23, which in turn is stabilized by additional hydrophobic interactions with aromatic side chains upstream in α1 (Figure S3-A). These structural features strongly suggest that conserved Phe27 is

placed immediately before the "hinge" to act as "hinge anchor" to preserve the structural integrity of α1 while the loop pivots between conformations. Phe46, located at the beginning of β2 near hinge residue Gly44, appears to fulfill a similar stabilizing role because its side chain packs against the side chain of conserved Tyr56; in turn, both aromatic side chains interact with the hemin in the holo-protein (Figure S3-B), which also suggests a role in stabilizing the heme complex.

Hemin binding is accompanied by a few relatively small but likely significant changes in the structure near the hemin binding site. Tyr75 is poised to coordinate the hemin-iron because its side chain undergoes minimal movement upon binding of hemin (Figure 2-C); motion of the His83 side chain reduces the distance to the phenol oxygen in Tyr75 from 3.3 Å to 2.6 Å, such that a relatively strong H-bonding interaction can be formed. Structural and spectroscopic investigations have determined this H-bonding interaction to be a conserved feature of hemin-bound hemophores,[10,12,45] which is thought to enhance the donating character of the phenolate ligand. In the apo-protein structure the side chain of Arg129 forms a H-bond with the side chain of Tyr138 in α2 (Figure 2-C). This interaction is lost upon hemin binding, as the side chain of Arg129 reorients to form a salt bridge with one of the hemin propionates; the side chain of Tyr138 moves to facilitate hemin binding and provide hydrophobic stabilization. Relocation of the Tyr138 side chain within hydrogen bonding distance (2.7 Å) of the coordinating His32 carbonyl oxygen suggests that this H-bond may help stabilize the His32 to iron coordination. The side chain of Met141, also located in α2, changes conformation upon hemin binding and interacts hydrophobically with the bound macrocycle, likely stabilizing the complex. Finally, when the His32 loop closes upon hemin binding, the carbonyl oxygen of Gly28 moves toward the short loop comprised of conserved Gly143 and Asp144, which connects α2 to α3. To accommodate the new conformation of the Gly28 hinge, the short loop relocates as depicted in Figure 2-D, which causes displacement in the carboxyl terminal of helix α2; this issue will be revisited later in this report. In comparison, motion of the other hinge residue (Gly45) can occur unimpeded by other structural elements in the hemophore.

The H32A Mutant of HasAp

When H32A apo-HasAp is reconstituted with hemin, followed by sieving the resultant solution through a Sephadex G-75 column, two peaks, each containing H32A holo-HasAp are obtained (Figure 4-A). The electronic absorption spectrum obtained from fractions corresponding to the fast-eluting peak exhibits a broad Soret band with maximum at 399 nm and peaks at 504 nm, 536 nm and 630 nm (black in Figure 4-B). In comparison, fractions corresponding to the slow-eluting peak exhibit spectra with a relatively narrower Soret band at 401 nm and peaks at 502 nm, 534 nm and 623 nm (red in Figure 4-B). The low-temperature resonance Raman spectra of these two fractions are very similar and exhibit porphyrin vibrations characteristic of high-spin ferric hemes. The coordination marker band v_3 suggests a predominantly 5-coordinate state in the first fraction while a greater contribution of 6-coordinate species exists in the second fraction (Figure S4). In the EPR spectra, both fractions exhibit intense g ~ 6 signatures consistent with axial S = 5/2 high iron (III) configurations, with evidence of signal broadening in the first fraction (Figure S5).

Analysis by SDS-PAGE indicated that protein from both peaks migrates at the same rate as the apo-protein, indicating that the different elution volumes from the Sephadex G-75 column are not due to degradation or covalent modification. To test the possibility that the two peaks eluting from the column may correspond to dimeric and monomeric H32A HasAp, protein eluting in each of the two peaks was loaded independently onto a calibrated, high resolution Superdex 75 column. Protein obtained from the fast-eluting peak in the Sephadex G-75 column exhibited an elution volume (V_e) of 13.2 ± 0.2 mL (red triangle in Figure 4-C), which corresponds to an estimated molecular mass of ~ 38.3 ± 2 kDa (dimer),

whereas protein from the slow-eluting peak exhibited V_e of 14.6 ± 0.1 mL (green diamond), which corresponds to $\sim 24.3 \pm 0.8$ kDa (monomer). The monomer and dimer H32A HasAp species are not in rapid dynamic equilibrium because once they have been separated, there is no indication of interconversion; *i.e.*, if either monomer or dimer protein is sieved again through a Sephadex G-75 column, the corresponding species elutes without evidence of interconversion. It is also important to note that the apo form of the H32A mutant elutes from the column in one single peak, with $V_e = 14.3 \pm 0.1$ (blue triangle) corresponding to an estimated molecular mass of $\sim 26.7 \pm 0.4$ kDa (monomer). Hence, dimerization of holo H32A HasAp is not a result of a pre-existing dimer population of the apo-protein, but a consequence of hemin uptake. Additional analysis revealed that the hemin to protein ratio in both the monomeric and dimeric species is 1:1, suggesting that the dimer consists of two holo-proteins, a hypothesis that was corroborated in the X-ray crystal structure of the dimer (see below).

Structural Characterization of H32A Holo-HasAp

A structure of H32A holo-HasAp was obtained from a sample that existed in a monomeric state. The structure, however, revealed a non-crystallographic dimer linked by cofacial interaction of two hemin molecules (Figure 5-A). The two hemin planes, defined by their corresponding pyrrole-nitrogen planes, intersect at an angle of 3.6°, and are separated by an average distance of ~3.4 Å, with approximately 60% overlap of the two macrocycles and an Fe to Fe distance of 5.51 Å. It is striking that the fold of each subunit is nearly identical to that of the apo-protein, including the conformation of the His32 loop (Figure 5-B). Coordination of the hemin iron in the proximal site is nearly indistinguishable from that observed in the wild type holo-protein, where the side chain of His83 is poised to accept a H-bond from the coordinating phenol oxygen of Tyr75. Both propionates in each of the hemin molecules adopt nearly identical H-bonding interactions with the protein; one of the propionates forms a H-bond to Arg129 from the subunit harboring it while the second propionate interacts with Tyr138 from the other subunit in the dimer. The in-plane orientation of the hemin in each of the subunits of the mutant is identical to that observed in wild type holo-HasAp, which allows conservation of the Arg129 to hemin propionate H-bond. Close inspection of the hemin molecules in the dimer makes it clear that there is no electron density between the two hemin planes that could be attributed to a bridging ligand (Figure 5-C), as would be the case if the dimer was linked by a μ-oxo ligand. In addition, the approximately 60% macrocycle overlap is in contrast to the nearly complete overlap in a μ-oxo dimer analogue.[46] Finally, the hemin-iron atoms in subunits A and B are displaced by 0.21 and 0.17 Å, respectively from the mean plane defined by the coordinating pyrrole-nitrogen atoms, toward the coordinating Tyr. This observation is consistent with a 5-coordinate iron, as observed in catalase[47] and a H93Y mutant of myoglobin.[48]

Figure 5-D, which shows subunit A in the dimer viewed from above the hemin (gold sticks), makes it evident that the macrocycle, in addition to being coordinated by the phenolate group of Tyr75, interacts hydrophobically with the side chains of Phe51, Tyr75, Leu76, Phe77 and His83 (green). With the exception of Phe51, the side chains that interact hydrophobically with hemin stem from residues located in the Tyr75 loop. This loop is nearly identical in the structures of the wt holo-, wt apo- and holo-H32A dimer molecules, suggesting that the invariant structure of the Tyr75 loop, in addition to poising the proximal Tyr75 ligand to coordinate the hemin iron, also functions by presenting a "sticky" hydrophobic surface that enables the hemophore to capture and retain the heme. Figure 5-D also shows that when the His32 loop (magenta) adopts the open conformation seen in the structure of the apo-protein, the distal face of the hemin is highly exposed to the aqueous environment. Hence, dimer formation is likely a mechanism whereby the exposed

hydrophobic surface of the hemin is satisfied by a cofacial interaction with a macrocycle from another hemophore molecule.

To investigate why crystals of dimeric H32A holo-HasAp are obtained from solutions containing monomeric protein, we tested the possibility that a component in the crystallization solution promotes dimerization. It was found that when monomeric holo H32A is dissolved in buffers containing ammonium sulfate at the same concentration as in the crystallization solution (1.26 M), the monomer is rapidly converted into a dimer, which is manifested in a near instantaneous change in the electronic absorption spectrum from that corresponding to the monomer (red in Figure 4-B) to that characteristic of the dimer (black trace). These observations indicate that ammonium sulfate in the crystallization solution promotes dimerization of the protein, prior to its crystallization. Ammonium sulfate is typically used to facilitate hydrophobic interactions and it is therefore likely that it exerts a similar influence on monomeric H32A holo-HasAp to facilitate the hydrophobic cofacial hemin interactions that stabilize the dimer. In this context, it is important to note that the structure of the dimer does not allow us to discern whether in solution the His32 loop in the hemin loaded monomeric mutant remains in the open conformation of the apo-protein, adopts a closed conformation similar to that seen in wt holo-HasAp, or, dynamically explores a range of conformations between the apo- and holo- structures. Because additional experiments aimed at finding conditions to crystallize the monomer were unsuccessful, this issue was explored by studying the imidazole complex of H32A holo-HasAp (H32A-imidazole); observations made with these experiments are described below.

The Imidazole Complex of Monomeric H32A Holo-HasAp

Titrating a solution containing monomeric H32A holo-HasAp with imidazole while monitoring the reaction with the aid of electronic absorption spectroscopy induces a shift of the Soret band from 402 nm to 407 nm (Figure S6-A). The latter value, which is in good agreement with the 407 nm exhibited by the Soret band in wild type holo-HasAp, strongly suggests the formation of a complex in which the heme is axially coordinated by Tyr75 and imidazole. The magnitude of the dissociation constant, $K_d = 4.7$ mM, was obtained by fitting the binding curve (Figure S6-B) to equation 1,[49] where [B] is the concentration of imidazole and AB/AB_{max} is the fraction of protein bound by imidazole. These observations indicated that although the complex is relatively weak, it is possible to obtain H32A HasAp fully bound by imidazole in the presence of relatively high concentrations of the ligand. Consequently, monomeric holo-HasAp in 150 mM imidazole buffer (pH 7.0) was used to screen crystallization conditions and to study the complex in solution with the aid of NMR spectroscopy.

$$\frac{AB}{AB_{max}} = \frac{[B]}{[B]+K_d}$$

Equation 1

X-ray Crystal Structure of the H32A-Imidazole Complex

Figure 6-A depicts the structure of H32A holo-HasAp in complex with imidazole, which overall is nearly identical to that of wt holo-HasAp. In the proximal side the heme-iron is coordinated by the phenol oxygen of Tyr75, which is 2.6 Å from the N_δ of His83, indicating that the role played by the latter in accepting a hydrogen bond from the coordinating Tyr75 phenol oxygen remains unchanged relative to the situation in wt holo-HasAp. In the distal side the heme-iron is coordinated by imidazole, the plane of which lies along the axis formed by the pyrrole I and pyrrole III nitrogens of the macrocycle. The His32 loop is not completely defined in the structure because residues 30–34 in molecule A of the non-

crystallographic dimer do not exhibit electron density and residues 31–36 are disordered in molecule B. Nevertheless, the segments of the loop with clearly discernible electron density exhibit conformations similar to those seen in corresponding sections of wt holo-HasAp. As indicated above, comparison of the apo- and holo-HasAp structures showed that the hinges about which the loop pivots from its "open" (apo) to its "closed" (holo) conformations are at Gly28 and at Gly45. In the structure of the H32A-imidazole complex the longest stretch of amino acid sequence exhibiting electron density in the His32 loop can be traced uninterrupted from one of the hinges (Gly45) to Val37. Only Gly28 and Asp29 are observable at the other hinge, but the conformations of these residues match the closed conformation in wt holo-HasAp. A zoomed in view of the loops is shown in Figure 6-B, where the structures of the wt (cyan) and H32A-imidazole (magenta) molecules are superposed. It is apparent that the hinges adopt their closed loop conformations and that the segments of the loop exhibiting electron density are structurally very similar to the corresponding stretches in the wild type protein. The coordinated imidazole in the H32A structure exhibits well-defined electron density (Figure 7-A) and its plane is nearly superimposable with the His32 imidazole plane in wt holo-HasAp (Figure 6-B). The well-defined electron density indicates that the imidazole ring is not rotating about the axis of the nitrogen-iron bond; rather, its rotation is restricted by a H-bond interaction with the carbonyl oxygen of Asn42 and by packing interactions with the side chains of Val38 and Met141 (Figure 7-B). Complimentary information in solution was obtained with the aid of NMR spectroscopy; results from these studies are presented below.

NMR Spectroscopic Characterization of the H32A HasAp Monomer in Solution

In an attempt to complement the X-ray structural studies we conducted investigations aimed at determining the topological location of the His32 loop in solution upon hemin binding. To this end monomeric H32A holo-HasAp and H32A-imidazole were studied in solution with the aid of NMR spectroscopy. Sequential backbone resonance assignments were obtained using a strategy similar to that employed for assigning backbone resonances in wt holo-HasAp,[12] which utilized conventional multidimensional heteronuclear experiments and selective amino acid labeling. This strategy allowed assignment of 125 and 154 non-proline amide cross-peaks for H32A HasAp and H32A-imidazole, respectively. Representative HSQC spectra obtained with samples of H32A HasAp and H32A-imidazole are shown in Figure S7 and the assignments are summarized in Tables S1 and S2. The extent of resonance assignment coverage in H32A HasAp, H32A-imidazole, and wt HasAp has been highlighted in gray in the structures of Figure 8; residues with missing assignments are highlighted in green. It is apparent that most of the unassigned residues in wt HasAp (Figure 8-C) are confined to the Tyr75 loop and a small portion of the His32 loop. That several residues in the Tyr75 loop lack assignments is due to their proximity to the hemin iron, which causes resonances to broaden beyond detection. In comparison, although several residues in the Tyr75 loops of H32A HasAp and H32A-imidazole are also unassigned for the same reason, there are other sections in these molecules with missing assignments: In H32A HasAp (Figure 8-A) these sections include the entirety of α2, the short loop connecting α2 to α3, the turn flanked by β3 and β4, and the C′-terminus of α1, whereas in H32A-imidazole a large portion of the His32 loop is unassigned (Figure 8-B). It is also important to note that although a relatively large number of residues have not been assigned in H32A HasAp, a majority of residues in its His32 loop have assignments, which is in contrast to the situation observed with H32A-imidazole, where a large portion of the His32 loop is unassigned. This contrasting accessibility to resonance assignments between H32A HasAp and H32A-imidazole is addressed below.

Conformational Exchange Distinctly Affects the Hinge Regions of H32A HasAp and H32A-Imidazole

The large conformational change of the His32 loop that occurs when wt apo-HasAp binds hemin pivots about hinge residues Gly28 (~157° about its φ angle) and Gly45 (~36° about its ψ angle). It is therefore interesting to note that dynamic processes affect these hinge regions in H32A HasAp and in H32A-imidazole differently: Near the Gly28 hinge, cross-peaks were not detected in the HSQC spectrum of H32A HasAp for Tyr26 and Phe27. In contrast, the corresponding cross-peaks in the spectrum of H32A-imidazole were readily identified because they exhibit cross-peaks with intensities similar to corresponding cross peaks in the spectrum of wt HasAp. At the other end of the loop, two of the three residues preceding the Gly45 hinge (Asn42 and Thr43) did not have detectable cross peaks in the HSQC spectrum of H32A HasAp or in the spectrum of H32A-imidazole. Gly44, on the other hand, gave rise to a cross-peak in the spectrum of uniformly labeled H32A HasAp (not shown) but was undetectable in the spectrum of uniformly labeled H32A-imidazole acquired with standard conditions (Figure 9-A). It was possible to observe the Gly44 amide cross-peak in H32A-imidazole only if HSQC spectra were acquired with fast repetition at 32 °C from a sample selectively labeled with ^{15}N-Gly (Figure 9-D). Observation of this cross-peak enabled its subsequent sequential assignment using data from the suite of 3-D spectra acquired with a sample uniformly labeled with ^{13}C and ^{15}N. Variable temperature studies revealed that below 32 °C the cross-peak is undetectable (Figures 9-B and C), it appears as a collection of low intensity cross-peaks in the spectrum obtained at 32 °C (Figure 9-D), and becomes more intense and likely dominated by a more abundant population at 38 °C (Figure 9-E). This temperature dependent behavior indicates conformational exchange affecting Gly44 in H32A-imidazole, which at the lower temperatures explored falls in the intermediate exchange regime, where exchange broadening renders the cross-peaks undetectable. At 32 °C the rate of exchange is accelerated and at least three populations (cross-peaks) can be observed; increasing the temperature to 38 °C causes the cross-peaks to migrate toward similar chemical shifts, resembling a single broad peak, which suggests that the distinct conformations seen at 32 °C are in rapid exchange with a thermally accessible state that becomes predominant at the higher temperatures. A similar, albeit less severe attenuation of intensity at low temperatures is observed for the cross-peak corresponding to Gly45 (Figure 9), indicating that this hinge residue is also affected by conformational exchange. The less pronounced attenuation of Gly45 peak intensity at the lower temperatures suggests that a lower energetic barrier separates the alternate conformations of Gly45 relative to Gly44. This is consistent with the notion that Gly45 is a hinge residue and is therefore less prone to explore large conformational rearrangements relative to Gly44.

Conformational Exchange Also Affects the Internal Regions of the His-32 Loop Differently in H32A-Imidazole and in H32A HasAp

As indicated above, most residues in the His32 loop of H32A-imidazole could not be assigned, whereas the similar stretch of sequence in H32A HasAp is nearly fully assigned (see Figure 8). This suggests that resonances from the His32 loop in H32A-imidazole are more affected by line broadening processes than equivalent resonances in H32A HasAp. To illustrate this point we describe key observations made from HSQC spectra acquired with standard and fast repetition rates from samples of H32A HasAp and H32A-imidazole labeled selectively with ^{15}N-Val: All valines in H32A HasAp were sequentially assigned from conventional 2D and 3D NMR data; cross-peaks corresponding to Val37 and Val38, located in the middle of the His32 loop are readily observed in HSQC spectra acquired with standard or with fast repetition conditions, Figure 10-A and 10-B, respectively. In comparison, only one of two cross peaks corresponding to Val37 and Val38 in H32A-imidazole could be observed in the HSQC spectrum of uniformly labeled protein acquired with standard conditions (not shown) or in the spectrum obtained with standard conditions

from a sample of ^{15}N-Val H32A-imidazole (Figure 10-C). When the HSQC spectrum is acquired with fast repetition conditions, however, two peaks are clearly observed in spectra obtained from uniformly labeled protein (not shown) or from a sample of ^{15}N-Val H32A-imidazole (Figure 10-D). Although these two cross peaks could not be sequentially assigned because correlations to neighboring carbon nuclei could not be found in 3D spectra, their presence in the HSQC spectrum of the ^{15}N-Val sample and the fact that all remaining Val residues had been assigned, allow us to confidently state that they originate from Val37 and Val38 in the His32 loop of H32A-imidazole. Given that protein concentrations were similar, the low intensity exhibited by the cross peaks corresponding to Val37 and Val38 in H32A-imidazole relative to their counterparts in the spectrum of H32A HasAp strongly suggests that conformational exchange differentially affects identical portions of the His32 loop in the two proteins. Moreover, the fact that the presence of imidazole bound to heme-iron directly influences the dynamic behavior of the Val37 and Val38 backbone is consistent with the packing interaction between Val38 and imidazole seen in the crystal structure (see Figure 7-B), thus supporting the idea that the conformation of the His32 loop in solution resembles more that observed in holo-HasAp than in its apo counterpart. In other words, the conformation adopted by the His32 loop in the crystal structure of H32A-imidazole is likely conserved in solution.

Targeted MD Simulations Suggest a Plausible Path for Closing the H32 Loop

Capitalizing from the availability of wt apo- and holo-HasAp structures we performed TMD simulations aimed at visualizing the closing of the His32 loop. As indicated in Experimental Methods, 25 independent 1.2-ns TMD simulations were carried out starting with the open loop (apo-structure) and ending with the closed loop (holo-structure). For each of the 25 independent simulations, 50 structures ("images") were generated at equal intervals of RMSD between the apo- and holo-structures; the images obtained at each RMSD for all 25 independent simulations were then clustered. Interestingly, the structural features of the image clusters at each RMSD are very similar, suggesting that the transition path between the open and closed states may be well defined. From this analysis a possible path for the conformational change exhibited by the His32 loop in going from apo- to holo-HasAp emerges. The path can be summarized in a minimalistic six-frame representation that conveys the most salient aspects of loop closing. The six frames are depicted in Figure 11-A to F, where the starting structure of apo-HasAp (gray) is overlapped with different structures (cyan) along the path of loop closing. In each frame key residues are highlighted in stick or CPK representation and when appropriate the same residues in the starting structure are shown in stick rendering for comparison between starting and intermediate structures. The peptide backbone RMSD between apo- and holo-HasAp at the start of the simulation is 5.73 Å.

Frame 11-A (RMSD 5.42 Å) shows that upon hemin binding helix α2 starts to tilt such that its C′-end begins to deviate from its position in the apo-structure. The motion of α2 also affects the short loop connecting α2 and α3, which moves outwards, thus breaking H-bonds between Gly143 (short loop) and Ser24 (α1). Binding of heme also causes β2, near the Gly45 hinge, to move away from the hemin, likely to avoid steric clashes between the side chain of Phe46 and the hemin. Frame 11-B (RMSD 4.87 Å) shows further tilting of α2 and displacement of the short loop connecting it to α3. The space open by the tilting of α2 allows the side chain of Phe27 (α1) to move downward and interact more efficiently with the side chains of Leu58 and Met141. It is likely that these attractive hydrophobic interactions provide the torque that causes helix α1 to undergo the observed bowing motion, which is also facilitated by the relocation of the short loop connecting α2 and α3. As α1 bows, the downward motion is transmitted to the turn connecting β3 and β4 (yellow) by the H-bonds between the carbonyl groups of Tyr26 and Phe27 in α1 and the hydroxyl groups of Ser60

and Ser63 in the turn. Frame 11-C (RMSD 4.06 Å) shows that the bowing motion of α1 pulls down a portion of the His32 loop near the Gly28 hinge. This in turn causes Val30, Val 37 and Val38, which in the apo structure interact with one another, to relocate near the yellow turn and interact with the backbone of the turn (Ser60 to Ser63), while residues next to Val30 and previous to Val38 interact with one another via H-bonds, as can be seen for Asn31 and Gly35 in this frame. These interactions appear to maintain the loop relatively organized as it slides over the yellow turn. It is important to underscore that the portion of the His32 loop between Gly28 and Val37 is the first section of the loop to start relocation. This is likely a direct consequence of the bowing motion of α1. In comparison, at this RMSD the remainder of the His32 loop maintains a structure similar to that of the apo-protein. Frame 11-D (RMSD 2.64) shows that the His32 loop continues to slide over the yellow turn; Val30, Val37 and Val38 re-establish a hydrophobic network, which by virtue of Leu58 is extended to encompass Phe27 and Met141 (not depicted in the frame). At the same time, Gln36 and Arg33 take their turn at interacting with the yellow turn. It is also noteworthy that α1 has relaxed back to near its original position, while the carbonyl group of Gly28 (hinge) has pivoted to attain its closed loop conformation; the tilting of α2 and concomitant displacement of the loop connecting it to α3 relax toward their initial position, but do not go back completely to provide the space necessary for the Gly28 carbonyl to adopt its closed loop conformation. Frame 11-E (RMSD 1.61 Å) shows that as Val37 and Val38 approach the heme the H-bond between Arg33 and Ala62 breaks, while the side chain of axial ligand His32 still points away from the heme. Analysis of motions between frame 11-E and frame 11-F (RMSD 0.61 Å) suggests that Arg33 explores different conformations until its guanidinium group forms a salt bridge with the carboxyl group of Asp29; this interactions appears to force the side chain of His32 to flip toward the heme, where it coordinates the iron, as can be seen in frame 11-F.

DISCUSSION

The X-ray structure of apo-HasAp reveals a fold very similar to that of holo-HasAp, except for the His32 bearing loop, which adopts a substantially different conformation and places the His32 axial ligand approximately 30 Å away from the hemin-iron (Figure 2). A similar open loop structure in apo HasAs led to the suggestion that hemin binds the hemophore in a two-step mechanism where the first interaction is with the Tyr75 loop, followed by closing and coordination of the His32 loop.[13] Additional observations have been interpreted as providing support for this notion: A crystal structure of HasAs bound to its receptor shows that the His32 ligand is not coordinated and the His32 loop is disordered;[15] when HasAs is reduced in the presence of CO the His32 rather than the Tyr75 ligand is replaced.[14] Although these observations taken together indicate a large conformational change for the His32 bearing loop and suggest that His32 may dissociate more readily than Tyr75 from the hemin-iron, the fact remains that conclusive evidence demonstrating that hemin is loaded first onto Tyr75 is lacking. Consequently, we conducted the investigations reported in reference[19] and herein with the aim of providing structural and spectroscopic evidence of possible intermediates in the process of hemin loading in HasAp. To this end we prepared His32A HasAp where the non-conserved His32 axial ligand is replaced by a non-coordinative residue, while leaving the axial Tyr75 and ancillary His83 ligands in the Tyr75 bearing loop intact. The apo form of the H32A mutant was determined to be monomeric in solution but a mixture of monomer and dimer after reconstitution with hemin. These two species, which can be separated by size exclusion chromatography, are not in dynamic equilibrium, so that once separated, there is no indication of monomer dimerization or dimer dissociation. Hence, the spectroscopic characteristics of each of the species could be ascertained unambiguously, which in turn allowed us to determine the nature of the oligomerization state in a sample simply on the basis of electronic absorption spectroscopy (Figure 4). The position of the Soret bands and the presence of high-spin marker bands

above 600 nm in the electronic absorption spectra indicate that the hemin-iron in the monomer and in the dimer are high-spin species. The resonance Raman spectra also support a high-spin heme iron(III) configuration, with the dimeric H32A HasAp preferentially adopting a 5-coordinate structure while the monomer consists of a mixture of 5- and 6-coordinate states. These spectroscopic approaches, however, did not provide information regarding the nature of the ligand(s) coordinating the hemin-iron in H32A HasAp; this issue was explored with the aid of X-ray crystallography.

Single crystals of H32A HasAp were grown from a solution of monomer; the structure, however, revealed a dimer linked by cofacial interactions of two hemin molecules (Figure 5). An interesting feature of this structure is the conformation of the His32 bearing loop, which is nearly identical to that adopted in the wt apo-protein, because it suggests that hemin binds to the Tyr75 bearing loop while the His32 bearing loop remains largely in its apo conformation. Once hemin is loaded on the Tyr75 loop, its proximal side is presumably rapidly coordinated by Tyr75, while its distal face remains largely exposed to the aqueous environment. Closing of the His32 loop would not only provide the sixth ligand but would also exclude water from the distal hemin face. In this context, cofacial macrocycle stabilization of the dimer may occur if two monomer molecules interact productively before the His32 loop approaches the distal face of the macrocycle and protects it. In agreement, kinetic studies comparing hemin loading into apo wt and H32A HasAp showed that initial loading of the hemin occurs in approximately 20 ms, producing a spectroscopic signature typical of 5-coordinate high spin hemin, which at 20 ms is identical for both wt and H32A HasAp. As time elapses the spectral signature of H32A HasAp remains unchanged while that corresponding to wt HasAp continues to evolve until the spectrum characteristic of holo HasAp is attained in approximately 1 sec.[19] Given that apo wt and H32A HasAp provide the same spectral signature at 20 ms, it was suggested that hemin is rapidly loaded into the Tyr75 loop while coordination of His32 occurs significantly more slowly. The structural data reported here provides direct experimental evidence that hemin does indeed bind to the Tyr75 loop to form a stable complex. Thus, a slow closure of the His32 loop during reconstitution can allow a subpopulation of proteins to dimerize in order to shield exposed hydrophobic surface in the hemin macrocycle and H32 loop from the aqueous environment. In this context, it is interesting that a bacterial protein involved in heme transport (chaN) in *Campylobacter jejuni* also undergoes dimerization via cofacial heme binding.[50] Hence, given that His32 is not conserved among the Has hemophores, our observations make it tempting to hypothesize that the dimer may be physiologically relevant in other bacterial species. It is also important to note that structural conservation of the Tyr75 loop in the apo- and holo-hemophore structures likely contributes to the hemin loading process in two important ways: (1) several side chains in the loop provide a "sticky" hydrophobic platform where the macrocycle can be captured (see Figure 5-D) and (2) the N_δ of His83 is poised to accept a H-bond from the phenol group in Tyr75, which facilitates coordination of the hemin-iron by a phenolate-like ligand.

The above discussion assumes that hemin binding triggers a conformational rearrangement of the A32 bearing loop which causes it to approach the macrocycle, thus shielding it from engaging in dimer-stabilizing cofacial interactions. The structure of the mutant dimer, however, shows that the A32 bearing loop remains very much like in the apo structure, and since this is likely a consequence of dimerization, it does not provide insight into the conformation of the loop in the monomer. Attempts to grow crystals of monomeric H32A HasAp were unsuccessful but its imidazole complex was crystallized successfully; the structure shows that the A32 bearing loop is located near the distal face of the macrocycle and that its conformation is very similar to that adopted by the His32 bearing loop in wt HasAp. This observation is in agreement with the idea that hemin loading in the Tyr75 loop triggers rearrangement of the A32 bearing loop. In solution the situation is apparently very

similar because the presence of imidazole causes significant changes in the properties of HSQC cross-peaks corresponding to residues in the A32 bearing loop: Whereas most of these loop resonances can be detected and sequentially assigned in the spectrum of H32A, as was the case for cross-peaks in the spectrum of the wt protein,[12] the corresponding resonances in the spectrum of the imidazole complex are mostly broadened beyond detection. Clearly, binding of imidazole alters the dynamic properties of residues in the A32 bearing loop, which we interpret to indicate that this segment of the structure is near the distal face of the heme, where it can interact with the coordinating imidazole. This last point is supported by the different dynamic behavior observed for Val37 and Val38 in the absence and presence of imidazole because this distict behavior is in agreement with the idea that the Ala32 loop in solution interacts with imidazole via Val38, as seen in the crystal structure, causing a change in the timescale of the motions affecting the loop.

We now direct attention to an important consequence of hemin loading onto the Tyr75 loop, which is to trigger the conformational rearrangement of the His32 loop. Comparison of sequential assignment coverage in H32A, wt and H32A-imidazole provides interesting insights. Figure 8-A shows that residues not assigned in H32A HasAp are located in the C′-terminal of α1, immediately previous to the Gly28 hinge, the entirety of α2, the short loop connecting α2 to α3, β2 at the Gly45 hinge, and the turn connecting β3 and β4. The difficulty in assigning the corresponding resonances arises mostly from peak broadening caused by dynamic processes affecting these sections of the holo-H32A structure. It is interesting that the same sections highlighted in green in Figure 8-A are implicated by the targeted MD simulations as undergoing motions important to the closing of the H32A bearing loop. In this context, it is interesting to hypothesize that in the absence of imidazole, the A32 bearing loop lacks stabilizing interactions needed to adopt stable conformations similar to that seen in the structure of the H32A-imidazole complex. Absence of these stabilizing interactions is manifested in dynamic processes affecting the hinge sections, as well as key portions of the structure associated with loop closing, which occur in a timescale that broadens the corresponding NMR signals so that they are either too weak to detect or to correlate sequentially. It is important to stress that the dynamic properties of these sections of the structure in relationship to closing of the H32 bearing loop have been independently inferred from the NMR spectroscopic studies in solution and from the targeted molecular dynamics simulations. This suggests that probing these sections of the hemophore structure may enable future investigations aimed at dissecting the mechanism of loop closing. In this frame, the insights obtained from analysis of the targeted MD simulations, which highlight important inter-residue interactions that appear to drive the motions of helices α2, α3 and the short loop connecting them may become a valuable guide for the design of mutant hemophore molecules with significantly altered kinetics of loop closing.

Supplementary Material

Refer to Web version on PubMed Central for supplementary material.

Acknowledgments

References

1. Bridges, KR.; Seligman, PA. Blood, Principles and Practice of Hematology. Handlin, RI.; Lux, SE.; Stossel, TP., editors. JB Lippincott Company; London: 1995. p. 1433-1472.

2. Ochsner UA, Johnson Z, Vasil ML. Microbiology. 2000; 146:185–198. [PubMed: 10658665]

3. Wandersman C, Delepelaire P. Annu Rev Microbiol. 2004; 58:611–647. [PubMed: 15487950]

4. Berka RM, Vasil ML. J Bacteriol. 1982; 152:239–245. [PubMed: 6811552]

5. Wandersman C, Stojiljkovic I. Curr Oppin Microbiology. 2000; 3:215–220.

6. Létoffé S, Ghigo JM, Wandersman C. Proc Natl Acad Sci USA. 1994; 91:9876–9880. [PubMed: 7937909]

7. Deniau C, Gilli R, Izadi-Pruneyre N, Lettofe S, Delepierre M, Wandersman C, Briand C, Lecroisey A. Biochemistry. 2003; 42:10627–10633. [PubMed: 12962486]

8. Ghigo JM, Léttofé S, Wandersman C. J Bacteriol. 1997; 179:3572–3579. [PubMed: 9171402]

9. Létoffé S, Redeker V, Wandersman C. Mol Microbiol. 1998; 28:1223–1224. [PubMed: 9680211]

10. Arnoux P, Haser R, Izadi N, Lecroisey A, Delepierre M, Wandersman C, Czjek M. Nature Structural Biology. 1999; 6:516–520.

11. Arnoux P, Haser R, Izadi-Pruneyre N, Lecroisey A, Czjek M. Proteins: Struct Funct Genet. 2000; 41:202–210. [PubMed: 10966573]

12. Alontaga AY, Rodríguez JC, Schönbrunn E, Becker A, Funke T, Yukl ET, Hayashi T, Stobaugh J, Moënne-Loccoz P, Rivera M. Biochemistry. 2009; 48:96–109. [PubMed: 19072037]

13. Wolff N, Izadi-Pruneyre N, Couprie J, Habeck M, Linge J, Rieping W, Wandersman C, Nilges M, Delepelairre P, Lecroisey A. J Mol Biol. 2008; 376:517–525. [PubMed: 18164722]

14. Lukat-Rodgers GS, Rodgers KR, Caillet-Saguy C, Izadi-Pruneyre N, Lecroisey A. Biochemistry. 2008; 47:2087–2098. [PubMed: 18205408]

15. Krieg S, Huché F, Diederichs K, Izadi-Pruneyre N, Lecroisey A, Wandersman C, Delepelaire P, Welte W. PNAS. 2009; 106:1045–1050. [PubMed: 19144921]

16. Lei B, Smoot LM, Menning HM, Voyich JM, Kala SV, DeLeo FR, Reid SD, Musser JM. Infect Immun. 2002; 2002:4494–4500. [PubMed: 12117961]

17. Aranda R, Worley CE, Liu M, Bitto E, Cates MS, Olson JS, Lei B, Phillips GN. J Mol Biol. 2007; 374:374–383. [PubMed: 17920629]

18. Nygaard TK, Blouin GC, Liu M, Fukumura M, Olson JS, Fabian M, Dooley DM, Lei B. J Biol Chem. 2006; 281:20761–20771. [PubMed: 16717094]

19. Yukl ET, Jepkorir G, Alontaga A, Pautsch L, Rodriguez JC, Rivera M, Moënne-Loccoz P. Submitted to Biochemistry. 2010

20. Rodríguez-Marañon MJ, Feng Q, Stark RE, White SP, Zhang X, Foundling SI, Rodríguez V, Schilling CL III, Bunce RA, Rivera M. Biochemistry. 1996; 35:16378–16390. [PubMed: 8973214]

21. Rodriguez JC, Wilks A, Rivera M. Biochemistry. 2006; 45:4578–4592. [PubMed: 16584193]

22. Alontaga AY, Bunce RA, Wilks A, Rivera M. Inorg Chem. 2006; 45:8876–8881. [PubMed: 17054345]

23. Wang A, Rodríguez JC, Han H, Schönbrunn E, Rivera M. Biochemistry. 2008; 47:8080–8093. [PubMed: 18605699]

24. Otwinowski, Z.; Minor, W. Methods in Enzymology, Macromolecular Crystallography, part A. Carter, CW.; Sweet, RM., editors. Vol. 276. Academic Press; New York: 1997. p. 307-326.

25. Kabsch W. Journal of Applied Crystallography. 1988; 21:67–72.

26. Evans P. Acta Cryst. 2006; D62:72–82.

27. Vagin A, Teplyakov A. J Appl Cryst. 1997; 30:1022–1025.

28. Langer G, Cohen SX, Lamzin VS, Perrakis A. Nat Protoc. 2008; 3:1171–1179. [PubMed: 18600222]

29. Murshudov GN, Vagin AA, Dodson EJ. Acta Crystallogr D Biol Crystallogr. 1997; 53:240–255. [PubMed: 15299926]

30. Adams PD, et al. Acta Cryst. 2010:D66.

31. Emsley P, Cowtan K. Acta Crystallogr D Biol Crystallogr. 2004; 60:2126–2132. [PubMed: 15572765]

32. Painter J, Merritt EA. Acta Crystallogr D Biol Crystallogr. 2006; 62:439–450. [PubMed: 16552146]

33. Lovell SC, Davis IW, Arendall WB 3rd, de Bakker PI, Word JM, Prisant MG, Richardson JS, Richardson DC. Proteins. 2003; 50:437–450. [PubMed: 12557186]

34. Potterton L, McNicholas S, Krissinel E, Gruber J, Cowtan K, Emsley P, Murshudov GN, Cohen S, Perrakis A, Noble M. Acta Crystallogr D Biol Crystallogr. 2004; 60:2288–2294. [PubMed: 15572783]

35. Harding MM. Acta Cryst. 2002; D58:872–874.

36. Delaglio F, Grzesiek S, Vuister GW, Zhu W, Pfeifer J, Bax A. J Biomol NMR. 1995; 6:277–293. [PubMed: 8520220]

37. Goddard, TD.; Kneller, DG. University of California. San Francisco:

38. Brooks BR, et al. J Comput Chem. 2009; 30:1545–1614. [PubMed: 19444816]

39. MacKerell AD Jr, et al. J Phys Chem B. 1998; 102:3586–3616.

40. Mackerell AD, Feig M, Brooks CL. J Comput Chem. 2004; 25:1400–1415. [PubMed: 15185334]

41. Jorgensen WL, Chandrasekhar J, Madura JD, Impey RW, Klein ML. J Chem Phys. 1983; 79:926–935.

42. Jo S, Kim T, Iyer VG, Im W. J Comput Chem. 2008; 29:1859–1865. [PubMed: 18351591]

43. Ryckaert JP, Ciccotti G, Berendsen HJC. J Comput Phys. 1977; 23:327–341.

44. Krissinel E, Henrick K. Acta Cryst. 2004; D60:2256–2268.

45. Caillet-Saguy C, Turano P, Piccioli M, Lukat-Rodgers GS, Czjzek M, Guigliarelli B, Izadi-Pruneyre N, Rodgers KR, Delepierre M, Lecroisey A. J Biol Chem. 2008; 283:5960–5970. [PubMed: 18162469]

46. Cheng L, Lee J, Powell DR, Richter-Addo GB. Acta Crystallog. 2004; E60:m1340–m1342.

47. Putnam CD, Arvai AS, Bourne Y, Tainer JA. J Mol Biol. 2000; 296:295–309. [PubMed: 10656833]

48. Hildebrand DP, Burk DL, Maurus R, Ferrer JC, Brayer GD, Mauk AG. Biochemistry. 1995; 34:1997–2005. [PubMed: 7849057]

49. Goodrich, JA.; Kugel, JF. Binding and Kinetics for Molecular Biologists. Cold Spring Harbor; New York: 2007.

50. Chan ACK, Lelj-Garolla B, Rosell FI, Pedersen KA, Mauk AG, Murphy MEP. J Mol Biol. 2006; 362:1108–1119. [PubMed: 16950397]

51. Larkin MA, Blackshields G, Brown NP, Chenna R, McGettigan PR, McWilliam H, Valentin F, Wallace IM, Wilm A, Lopez R, Thompson JD, Gibson TJ, Higgins DG. Bioinformatics. 2007; 23:2947–2948. [PubMed: 17846036]
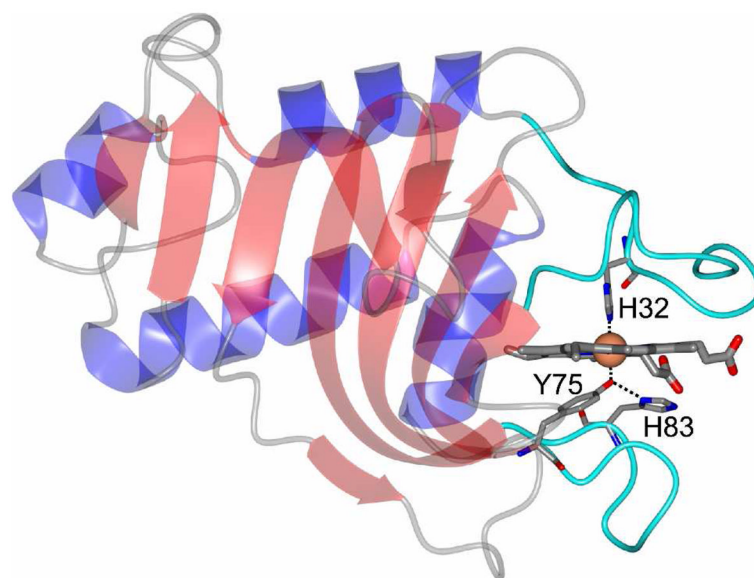
Figure 1.
Holo HasAp (PDB: 3ELL) showing the "α-helix wall" (blue) and "β-sheet wall" (red). The two extended loops containing the residues that coordinate the hemin iron are colored turquoise. Specific residues involved in the coordination of the heme are indicated.
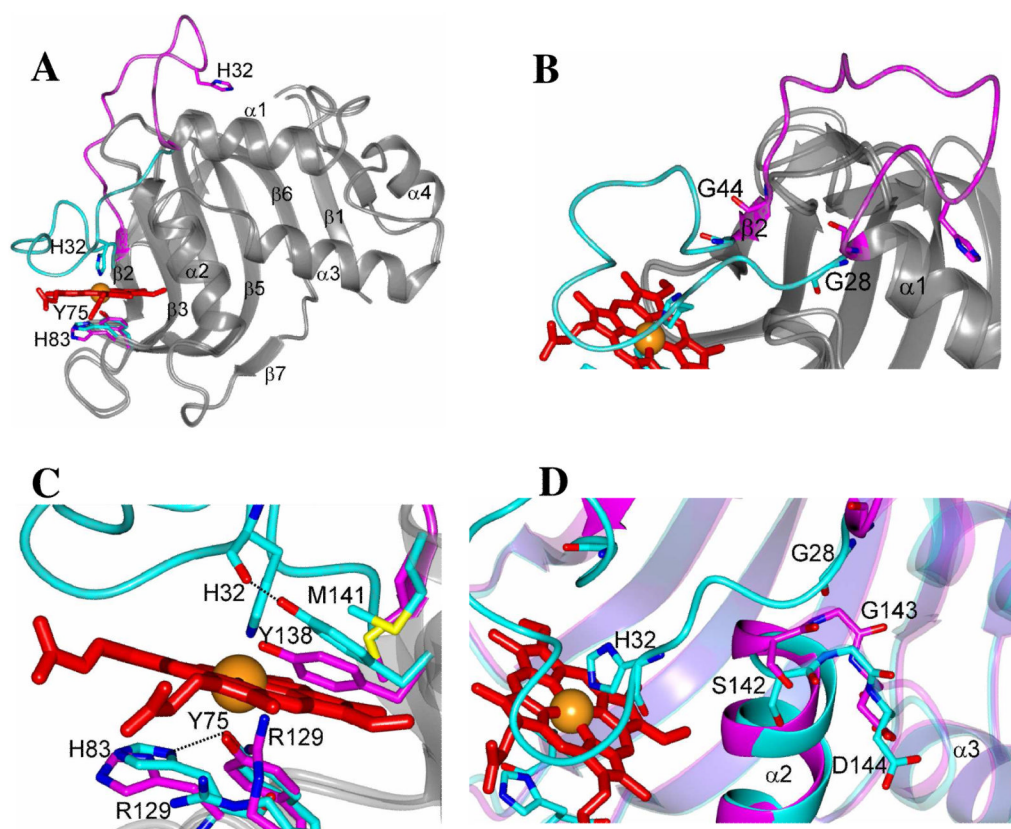
Figure 2.
Overlay of apo (magenta) and holo (turquoise, PDB: 3ELL) HasAp. A) Conformational changes in the His32 bearing loop between G28 and G44; secondary structure elements are indicated. B) Zoomed in view of the "hinge" region of the His32 bearing loop. C) Zoomed in view of the heme binding pocket showing conformational differences between certain residues upon hemin binding. D) Displacement of helix α2 and the short loop comprised by G143 and D144 relative to the apo-protein upon hemin binding; movement of the latter enables hinge residue G28 in the holo structure to adopt its hemin bound conformation.

```
                10        20        30        40        50        60
                 |         |         |         |         |         |
      Pa  MSISISYSTTYSGWTVADYLADWSAYFGDVNHRPGQVV-DGSNTGGFNPGP--FDGSQYALKS-TASDAAFIA
      Sm  MAFSVNYDSSFGGYSIHDYLGQWASTFGDVNHTNGN-V-TDANSGGFYGGS--LSGSQYAISSTANQVTAFVA
      Pe  MTISVNYDAAFASSTIDDYLAFWSAGFVTAGHG-------YSNTGGFSNGT--YDGDQYATHGRNSSDYAFIA
      Pf  MSISISYSATYGGNTVAQYLTDWSAYFGDVNHRPGEVV-DGTNTGGFNPGP--FDGTQYAIKS-TASDAAFVA
      Yps MSTTIQYNSNYADYSISSYLREWANNFGDIDQAPAETK----DRGSFSGSSTLFSGTQYAIGSSHGNPEGMIA
      Pc  MSFAITYDAYYANYSIASYLTEWSAAFGDVNHTAGNTQVGGNNTGGFYGGDTFIDGTQYAITSTQNDFSALIA
      Ec  MSFAITYDAYYANYSIANYLTEWSAAFGDVNHTTGNTQVGGNNTGGFYGGDTFIDGSQYAITSTQNDFSALIA
      Yp  MSTTIQYNSNYADYSISSYLREWANNFGDIDQAPAETK----DRGSFSGSSTLFSGTQYAIGSSHSNPEGMIA
      Ypa MSTTIQYNSNYADYSISSYLREWANNFGDIDQAPAETK----DRGSFSGSSTLFSGTQYAIGSSHSNPEGMIA

                70        80        90       100       110       120
                 |         |         |         |         |         |
      Pa  GGD----LHYTLFS------NPSHTLWGKLDSIALGDTLT---GGASSGG-YALDSQEVSFSNLGLDSPIAQ-
      Sm  GGN----LTYTLFN------EPAHTLYGQLDSLSFGDGLS---GGDTSP--YSIQVPDVSFGGLNLSSLQAQ-
      Pe  DSNNANGLHYVFDPSKAPGDNLNHYLWGSLDNVSLGEVLG---GGSGSD--FTLGNYVVNFNGLDLDAAHGA-
      Pf  DGN----LHYTLFS------NPSHTLWGSVDTISLGDTLA---GGSGSN--YNLVSQEVSFTNLGLNSLKEE-
      Yps EGN----LKYSFM--------PQHTFYGQIDTLQFGKDLATNAGGPSAG--KHLEKIDITFNELDLSGEFDSG
      Pc  GGD----LTYSLFT------PPAHTLYGDLDSLSFGNVLQ---GGTTAGTTYSLAEPEVTFSGLDLSTDVAN-
      Ec  GGD----LTYSLFS------PPAHTLYGDLDSLSFGNVLQ---GGTTAGTTYSLVEPEVTFSGLDLSTDVAN-
      Yp  EGD----LKYSFM--------PQHTFHGQIDTLQFGKDLATNAGGPSAG--KHLEKIDITFNELDLSGEFDSG
      Ypa EGD----LKYSFM--------PQHTFHGQIDTLQFGKDLATNAGGPSAG--KHLEKIDITFNELDLSGEFDSG

                130       140       150       160       170       180       190
                 |         |         |         |         |         |         |
      Pa  ---GR-DG-TVHKVVYGLMSGDSSALQGQIDALLKAVDPSLSINSTFDQLAAAGVAHATP-AAAAAEVGVVGV
      Sm  ---GH-DG-VVHQVVYGLMSGDTGALETALNGILDDYG--LSVNSTFDQVAAA----T-----------AVGV
      Pe  ---GR-AGNEVQTVIYGLMQGNTAGLEGVLDTLLASYG--VSTNDTFDVVAAA----LGG-ASGAASAQAVGV
      Pf  ---GR-AG-EVHKVVYGLMSGDSSALAGEIDALLKAIDPSLSVNSTFDDLAAAGVAHVNPAAAAAADVGLVGV
      Yps KSMTENHQGDMHKAILGLRKGNA----DPMLEVMKAKG--FDVDTAFKDLSIASQYPDSGYMSDAPMVDTVGV
      Pc  --LTVSDRGVVHDVIYGLMSGQV----QPLLDALTNAG--IDINASLDSLSFATATSDAALSADT-VVDVVGV
      Ec  --LTVSDRGVVHDVIYGLMGGQV----QPLLDALTNAG--IDINASLDSLSFATATSDAALSADT-VVDVVGV
      Yp  KSMTENHQGDMHKSVRGLMKGNP----DPMLEVMKAKG--INVDTAFKDLSIASQYPDSGYMSDAPMVDTVGV
      Ypa KSMTENHQGDMHKSVRGLMKGNP----DPMLEVMKAKG--INVDTAFKDLSIASQYPDSGYMSDAPMVDTVGV

                200   205
                 |     |
      Pa  QELPHDLALAA
      Sm  QHADSPELLAA
      Pe  QALPEDLALAA
      Pf  QDVAQDWALAA
      Yps MDSN-DMLLAA
      Pc  AETA-DLLAA-
      Ec  AETA-DLLAA-
      Yp  VDCH-DMLLAA
      Ypa VDCH-DMLLAA
```
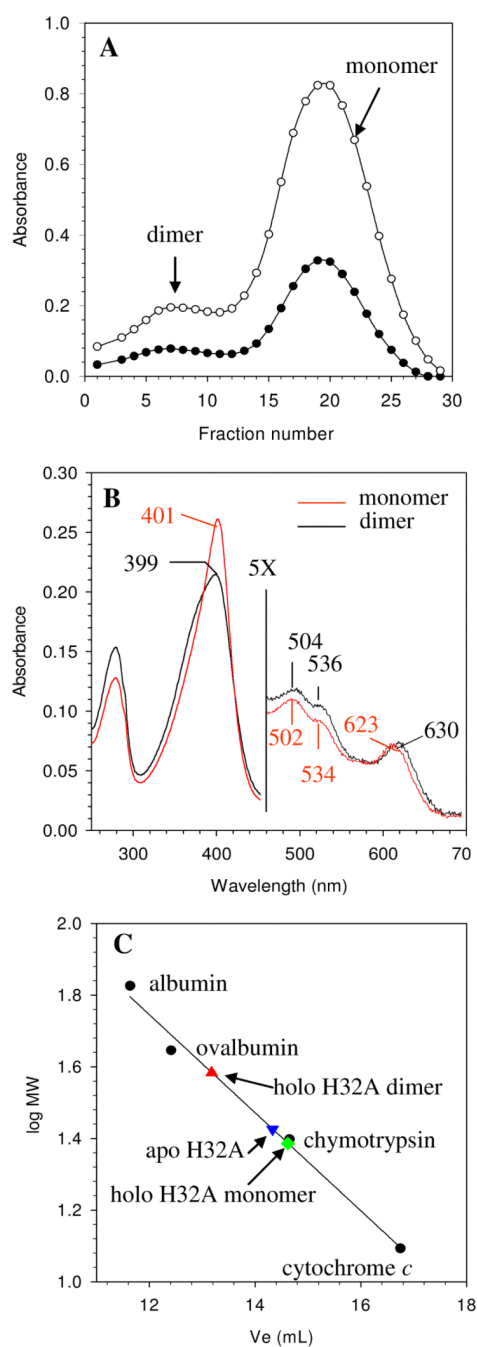
Figure 3.
Amino acid sequence alignment of full-length HasA sequences from *P. aeruginosa* (Pa), *Serratia marcescens* (Sm), *P. entomophila* (Pe), *P. fluorescens* (Pf), *Yersinia pseudotuberculosis* (Yps), *Pectobacterium carotovorum* (Pc), *Erwinia carotovora* (Ec), *Yersinia Pestis* (Yp), and *Yersinia Pestis bv. Antiqua* (Ypa), aligned against the sequence of HasA from *P. aeruginosa*. Truncated HasAp used in these investigations stops at residue 184 (full-length minus 21 amino acids).[12] Residues highlighted in red are conserved while those in blue are the His32 loop "hinge" residues in HasAp. The alignment was performed using ClustalW.[51]

Figure 4.
(A) Elution profile of H32A holo-HasAp from a Sephadex G-75 column; open circles track the Soret band absorption (~ A_{400} nm) and black circles track A_{280} nm. (B) Black: Electronic absorption spectra of fractions in the fast eluting peak (dimer); red: spectra of fractions in the slow eluting peak (monomer). The ratio of dimer to monomer obtained under these conditions (see Experimental) is ~ 15%). (C) Elution volumes (V_e) from a calibrated Superdex 75 column and estimated molecular weights for: (♦) monomer holo H32A HasAp, (▲) dimer holo H32A HasAp, and (▼) apo H32A HasAp; the average molecular weight was obtained from two experiments. The Superdex 75 column was calibrated with (•) albumin (67 kDa), ovalbumin (44 kDa), chymotrypsin (25 kDa), and cytochrome c (12.4 kDa).
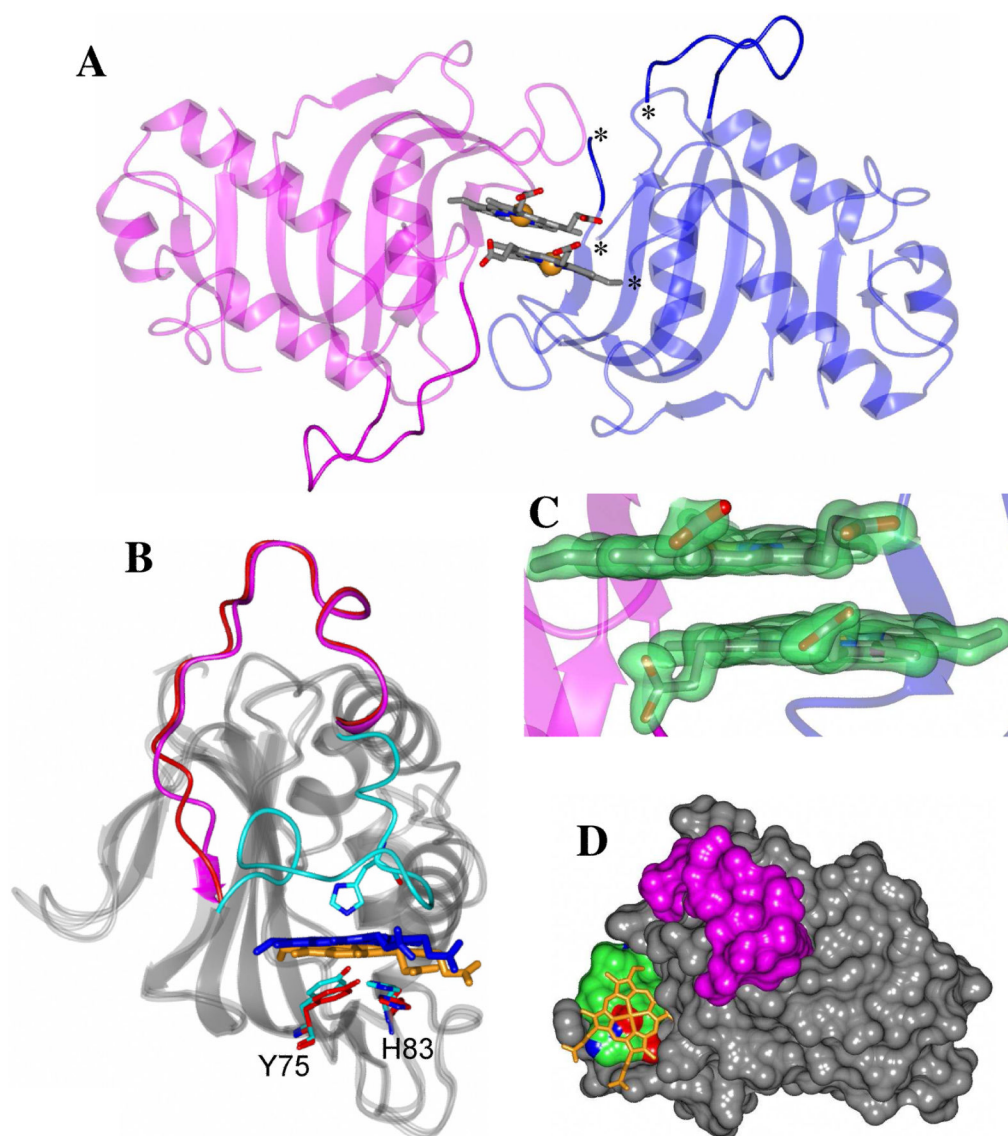
Figure 5.
Structure of the H32A holo-HasAp dimer. A) Subunits A and B are colored magenta and blue respectively; the H32 loops are highlighted darker; disordered residues in subunit B are located between the asterisks. B) Overlay comparing the H32 loops of apo wt (magenta), holo wt (cyan) and holo H32A (red) HasAp. The hemin molecules associated with holo wt and holo H32A are colored blue and gold, respectively. C) 2Fo-Fc electron density maps of the hemin molecules contoured at 1σ are represented as a green surface. D) Surface representation of subunit A and associated hemin (gold). The H32 loop is colored magenta and hydrophobic residues Phe51, Tyr75, Leu76, Phe77 and His83 in the hemin binding site are colored green.
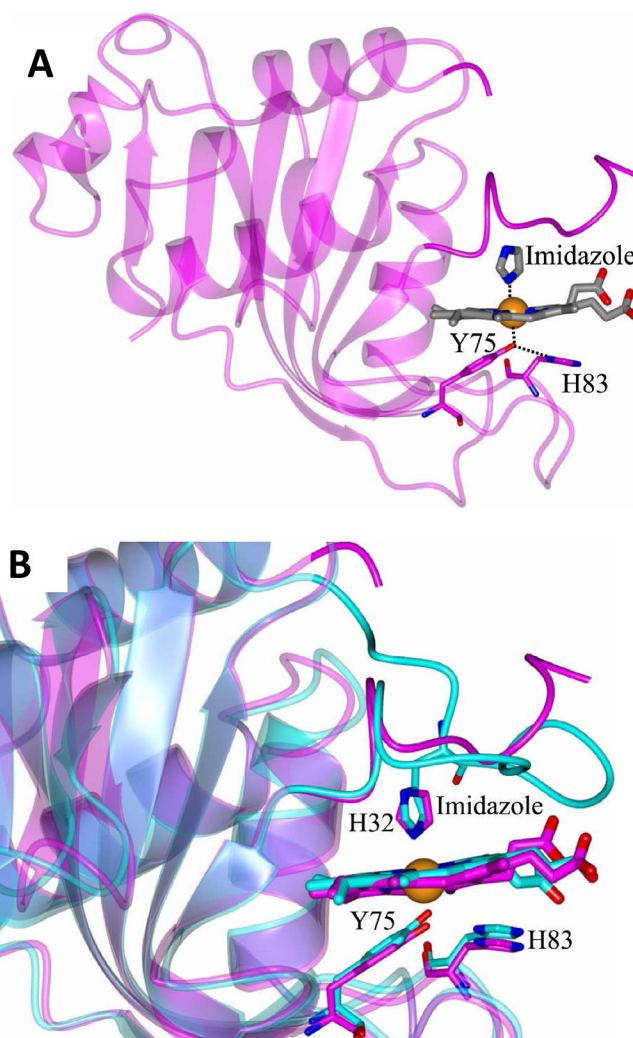
Figure 6.
(A) Molecule A of the H32A-imidazole complex. Residues in the H32 loop are colored darker. (B) Superposition of molecule A of the H32A-imidazole complex (magenta) with molecule A of wt holo-HasAp (cyan). Residues in the H32 loop are colored darker.
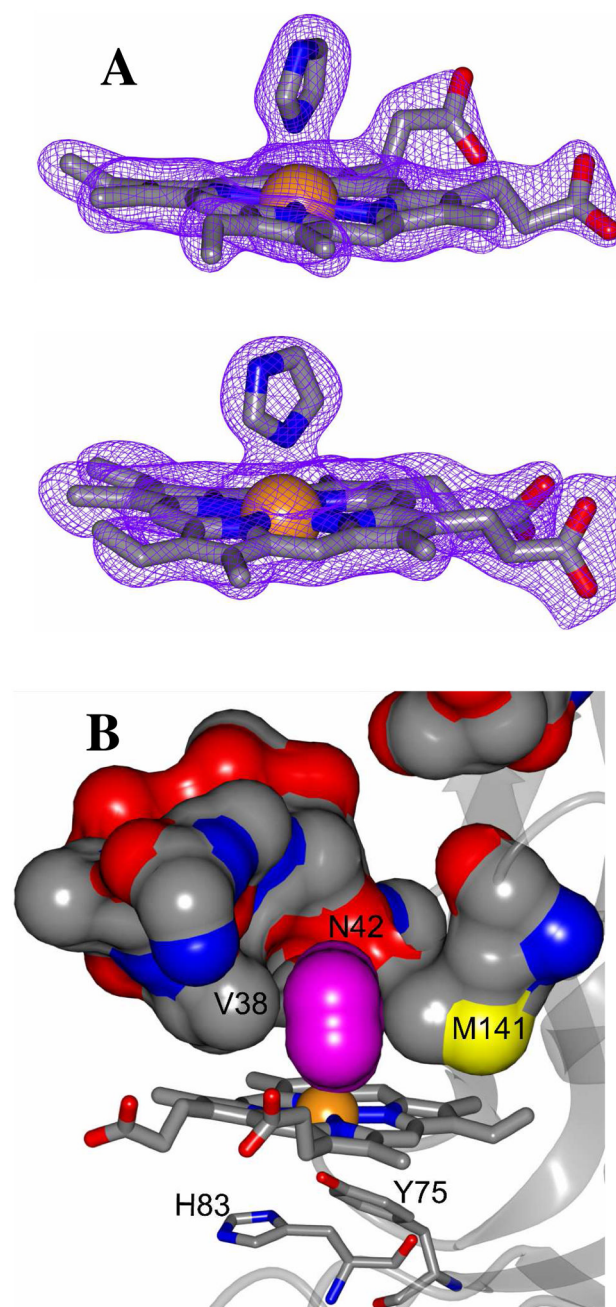
Figure 7.
(A) 2Fo-Fc electron density maps of the hemin and hemin-bound imidazole in molecule A (top) and molecule B (bottom) of the H32A-imidazole complex contoured at 1σ. (B) Surface representation of the H32 loop in the structure of the H32A-imidazole complex. The imidazole molecule (magenta) is locked in place by the Val38 and Met141 side chains, and a hydrogen bond formed with the carbonyl oxygen of Asn42.
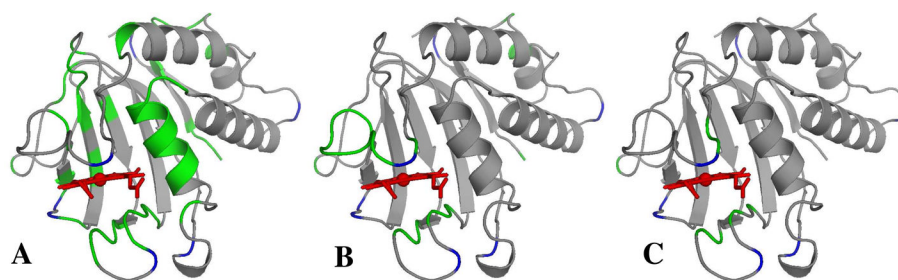
Figure 8.
Resonance assignments available for H32A HasAp (A), H32A-imidazole (B) and wt HasAp (C) are mapped in gray on the structure of wt holo-HasAp; residues for which resonances could not be obtained are shown in green, prolines are in blue and the hemin is in red.
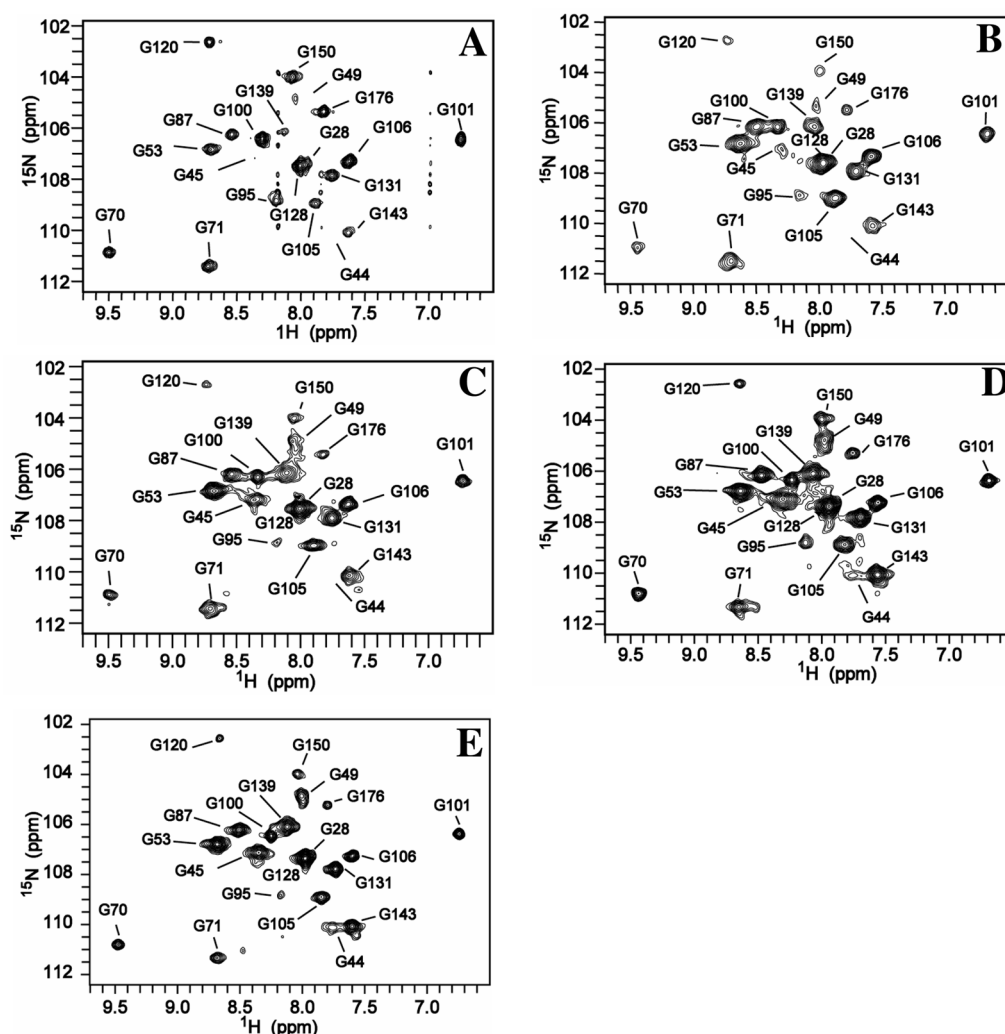
Figure 9.
HSQC spectra obtained with samples of ^{15}N-Gly-H32A-imidazole using standard (A) and fast-repetition (B–E) conditions. Spectra were taken at 32 °C (A and D), 15 °C (B), 25 °C (C) and 38 °C (E). Cross-peaks are labeled according to the corresponding sequential assignment. The cross-peak identified as Gly44 is observed only in spectra collected at 32 °C and 38 °C using a short relaxation delay (50 ms) and short acquisition time (35 ms). The spectra were recorded with 100 increments in t_1 (^{15}N); 630 complex points in t_2 (^{1}H), over a spectral width of 8.9 kHz (^{1}H) and 2.3 kHz (^{15}N), with 256 scans per increment for all temperatures except 15 °C, for which 512 scans were used. The data were processed using NMRPipe applying a 90°-shifted squared sine bell apodization function in each dimension, followed by zero filling to 4k data points in t_2, and linear prediction to twice the number of points and zero filling to 4k data points in t_1. Subsequent Fourier transformation and phasing rendered matrices of 4k × 4k points.
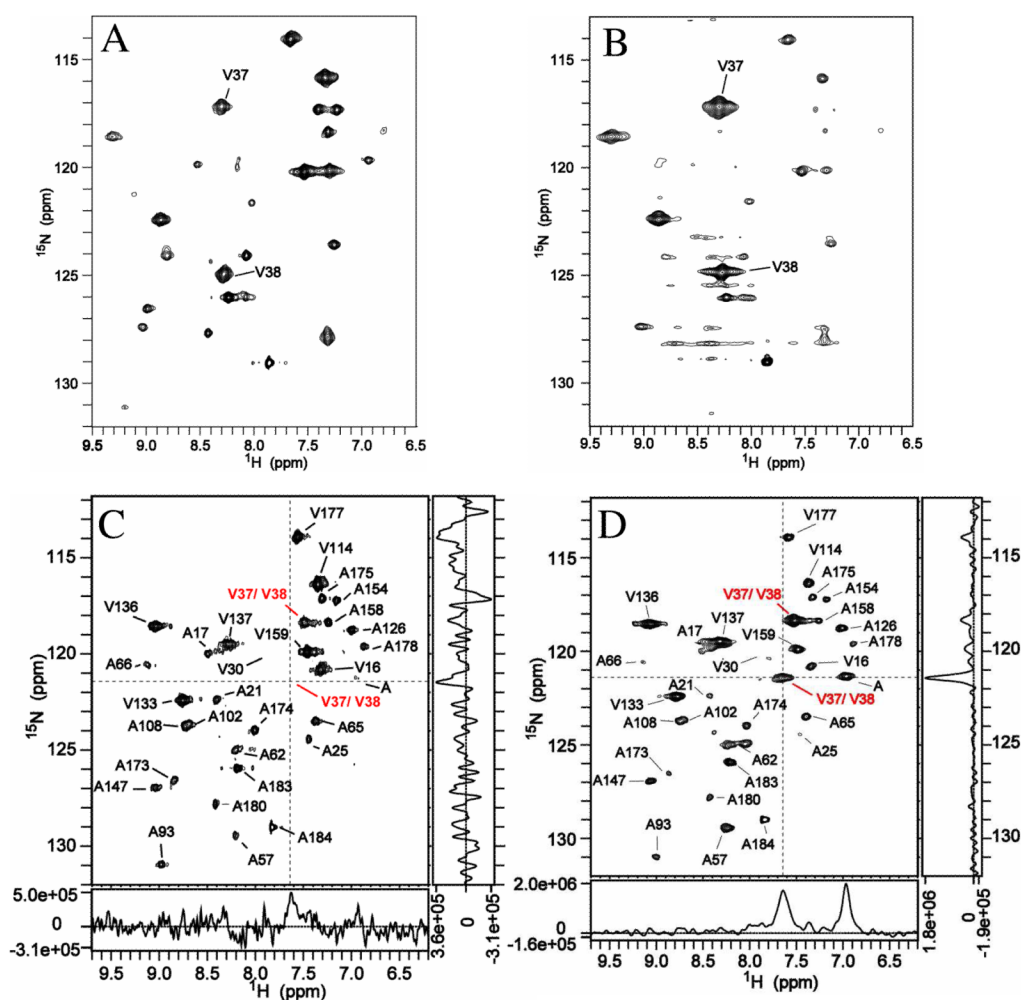
Figure 10.
HSQC spectra obtained with samples of ^{15}N-Val-H32A HasAp (A and B) and ^{15}N-Val-H32A-imidazole (C and D). Spectra in (A) and(C) were acquired with standard acquisition parameters, whereas spectra in (B) and (D) were collected with fast-repetition conditions. Dashed lines in spectra (C) and (D) highlight one of the cross-peaks attributed to Val37 or Val38, which is clearly visible only in the HSQC spectrum (and corresponding 1D trace) acquired with fast repetition conditions. Cross-peaks are labeled according to their sequential assignment. Cross-peaks originating from backbone amides of Ala residues are present because of isotopic scrambling, and are clearly identified by comparison with the HSQC spectrum obtained with uniformly labeled protein.
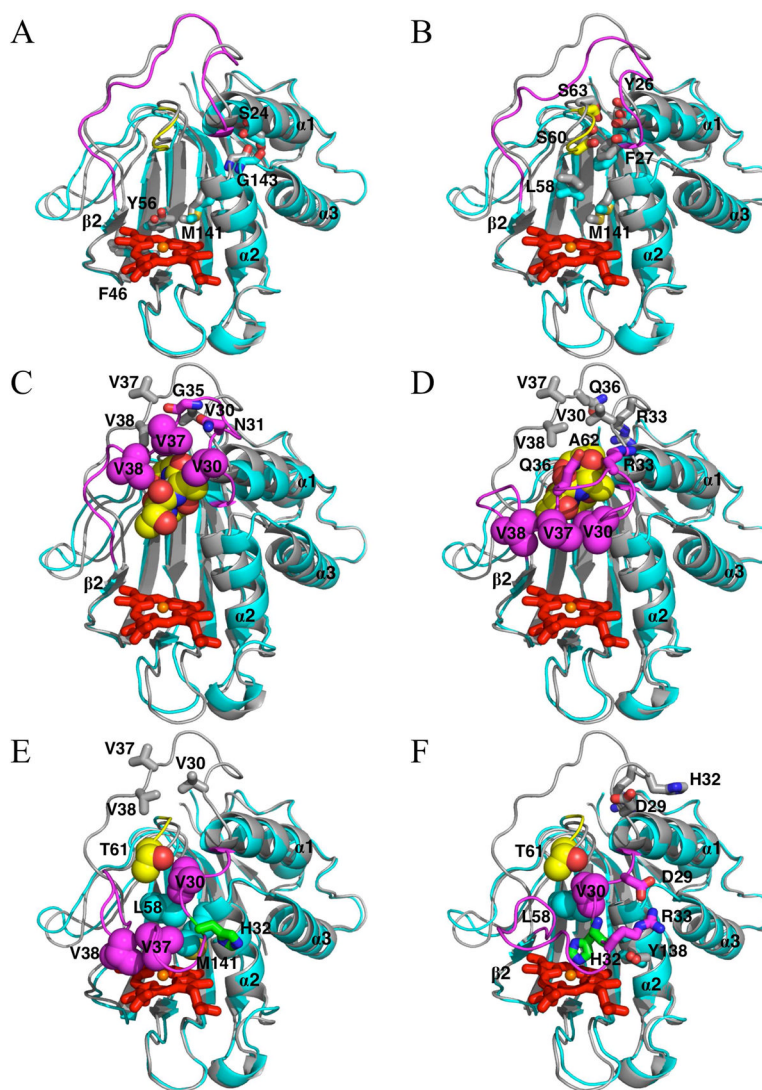
Figure 11.
A possible path for closing of the H32 loop upon hemin binding; the heavy atom RMSD between initial (apo-) and final (holo-) structures is 5.73 Å, including snapshots at RMSD 5.42 Å (A), 5.87 Å (B), 4.06 Å (C), 2.64 Å (D), 1.61 Å (E) and 0.61 Å (F). The apo- (grey) and intermediate (cyan) structures are shown in cartoon representation. Residues involved in important interactions are shown in either stick or sphere representation and when appropriate, the same residues in the apo-structure are also shown to indicate their initial positions. The His32 loop and the turn (Ser60 to Ser63) are highlighted in magenta and yellow, respectively. The hemin and hemin-iron are shown as red sticks and orange sphere, respectively.

Table 1

Crystallographic data of HasAp structures.

	Apo-HasAp	HasAp H32A Dimer	HasAp H32A Imidazole
Data Collection			
Unit-cell parameters (Å,°)	$a = 32.98$, $b = 65.25$, $c = 38.34$, $\beta = 110.5$	$a = 71.74$ Å, $b = 52.70$ Å, $c = 85.71$ Å, $\beta = 91.48$	$a = 41.37$ Å, $b = 46.38$ Å, $c = 81.09$ Å, $\beta = 97.01$
Space group	$P2_1$	$I2$	$P2$
Resolution (Å)[i]	50.0-1.55 (1.61 - 1.55)	50.0-1.20 (1.30-1.20)	30.0-2.25 (2.33-2.25)
Wavelength (Å)	1.0000	1.0000	1.5418
Observed reflections	78,274	443,848	47,076
Unique reflections	21,268	95,175	16,389
$\langle I/\sigma(I)\rangle$[1]	22.9 (2.1)	17.0 (3.4)	15.6 (2.3)
Completeness (%)[i]	98.5 (72.4)	95.0 (91.9)	96.6 (91.8)
Redundancy[i]	3.7 (2.1)	4.7 (3.5)	2.9 (2.6)
R_{sym}[i,ii]	7.6 (32.3)	4.1 (35.0)	411.6 (53.5)
Refinement			
Resolution (Å)	35.92-1.55	19.25-1.20	24.65-2.25
Reflections (working/test)	20,125/1,095	87,374/4,379	15,450/821
R_{factor}/R_{free} (%)[iii]	15.3/17.8	17.7/19.7	21.4/26.7
No. of atoms protein (chain A, B)/heme/water)	1344/-/158	1353, 1273/86/305	1259, 1269/86/64
Model Quality			
R.m.s deviations			
Bond lengths (Å)	0.014	0.010	0.018
Bond angles (°)	1.434	1.421	1.617
Average B factor (Å^2)			
All Atoms	15.7	21.5	42.3
Protein	15.4	14.9/27.7	40.4/44.9
Water	25.8	25.7	36.8
Heme	-	20.7	35.6
Phosphate or imidazole	26.0	-	41.9
Coordinate error based on maximum likelihood (Å)	0.05	0.16	0.21
Ramachandran Plot			
Most favored (%)	97.3	97.2	95.9
Additionally allowed (%)	2.2	2.2	4.1
Disallowed (%)	0.5	0.4	

[i]Values in parenthesis are for the highest resolution shell.

[ii]$R_{sym} = \Sigma_{hkl}\Sigma_i |I_i(hkl) - \langle I(hkl)\rangle|/\Sigma_{hkl}\Sigma_i I_i(hkl)$, where $I_i(hkl)$ is the intensity measured for the ith reflection and $\langle I(hkl)\rangle$ is the average intensity of all reflections with indices hkl.

[iii]$R_{factor} = \Sigma_{hkl} ||F_{obs}(hkl)| - |F_{calc}(hkl)||/\Sigma_{hkl} |F_{obs}(hkl)|$; Rfree is calculated in an identical manner using 5% of randomly selected reflections that were not included in the refinement.